A ^{29}Si MAS NMR Spin-Lattice Relaxation Study of Paramagnetics-Doped Orthosilicates

by

David R. Sliwinski, B.Sc. Honours Chem., Brock

A Thesis

submitted to the Department of Chemistry

in partial fulfillment of the requirements

for the degree of

Master of Science

July 1991

Brock University

St. Catharines, Ontario

ABSTRACT

A ^{29}Si MAS NMR study of spin-lattice relaxation behaviour in paramagnetic-doped crystalline silicates was undertaken, using synthetic magnesium orthosilicate (forsterite) and synthetic zinc orthosilicate (willemite) doped with 0.1% to 20% of Co(II), Ni(II), or Cu(II), as experimental systems. All of the samples studied exhibited a longitudinal magnetization return to the Boltzmann distribution of nuclear spin states which followed a stretched-exponential function of time:

$$Y=\exp[-(t/T_n)^n],\ 0<n<1$$

For the most reliable experimental data, there is a bias toward n=0.5; the few genuine cases of deviation from 1/2-power are for dopant concentrations equal to or exceeding 2.5 percent dopant.

In some cases we find agreement with theory, and observe a direct proportionality between the spin-lattice relaxation time and paramagnetic dopant ion concentration, with $T_{ni}[M^{2+}]_i=T_{nj}[M^{2+}]_j$ for a given dopant and mineral. There are many cases where this correlation is not apparent, however, and this is attributed to the structural,phase, and ion distribution complexities inherent in many of these systems.

ACKNOWLEDGEMENTS

Appreciation must be extended to my co-supervisors, Professors J.S. Hartman and E.A. Cherniak, for all of the time and effort which they invested in this project. Thanks also to the electronics and machine shop staffs who laboured for many hours on my behalf. I wish to acknowledge the equipment and advice freely given by Professor F.P. Koffyberg. Sincere gratitude goes to T. Jones and D. Vukmanic for helping to smooth out many of the technical wrinkles. Thanks to R. Millard, M. Seifried, S. Rigby and the students of the chemistry 3P31 lab for assistance in sample preparation. Thanks to Professor I.D. Brindle for providing access to the DCP spectrometer, to Brian Sayer for helping with the NMR work at McMaster, and to Neil Ball at the University of Manitoba for running the XRD spectra. Finally, thanks to my co-workers for their timely assistance and encouragement.

TABLE OF CONTENTS

Experimental

Results

Discussion

LIST OF TABLES

LIST OF ILLUSTRATIONS

INTRODUCTION

(A) Nuclear Magnetic Resonance

Nuclear magnetic resonance spectroscopy owes its existence to the fact that many nuclei have quantized spin states. In the absence of an external magnetic field, the energy of these spin states is the same, and we say that they are degenerate. On applying a magnetic field to the nuclear population, the degeneracy is split (see Figure 1). Spin states in which the nuclear magnetic moment (arising from the spinning of a charged nucleus) has a component parallel to the external field attain a lower energy; where the nuclear magnetic moment has a component antiparallel to the external field, the energy will be increased. The magnitude of energy decrease or increase is the same for states with the same spin quantum numbers, for a given nucleus. The energy gap between spin states is directly proportional to the strength of the external magnetic field being applied.

When a nuclear population exhibits two or more spin states with different energies, the potential exists for performing energy absorption and/or emission studies. In the case of NMR, the photons involved fall into the radio frequency band, due to the tiny amounts of energy involved.

The frequency of absorption depends on an innate property of the nucleus known as the gyromagnetic ratio.

$$\nu = \frac{\gamma B_o}{2\pi} \qquad (1)$$

FIGURE 1

The energy levels of I = 1/2 and I = 1 nuclei are illustrated here.

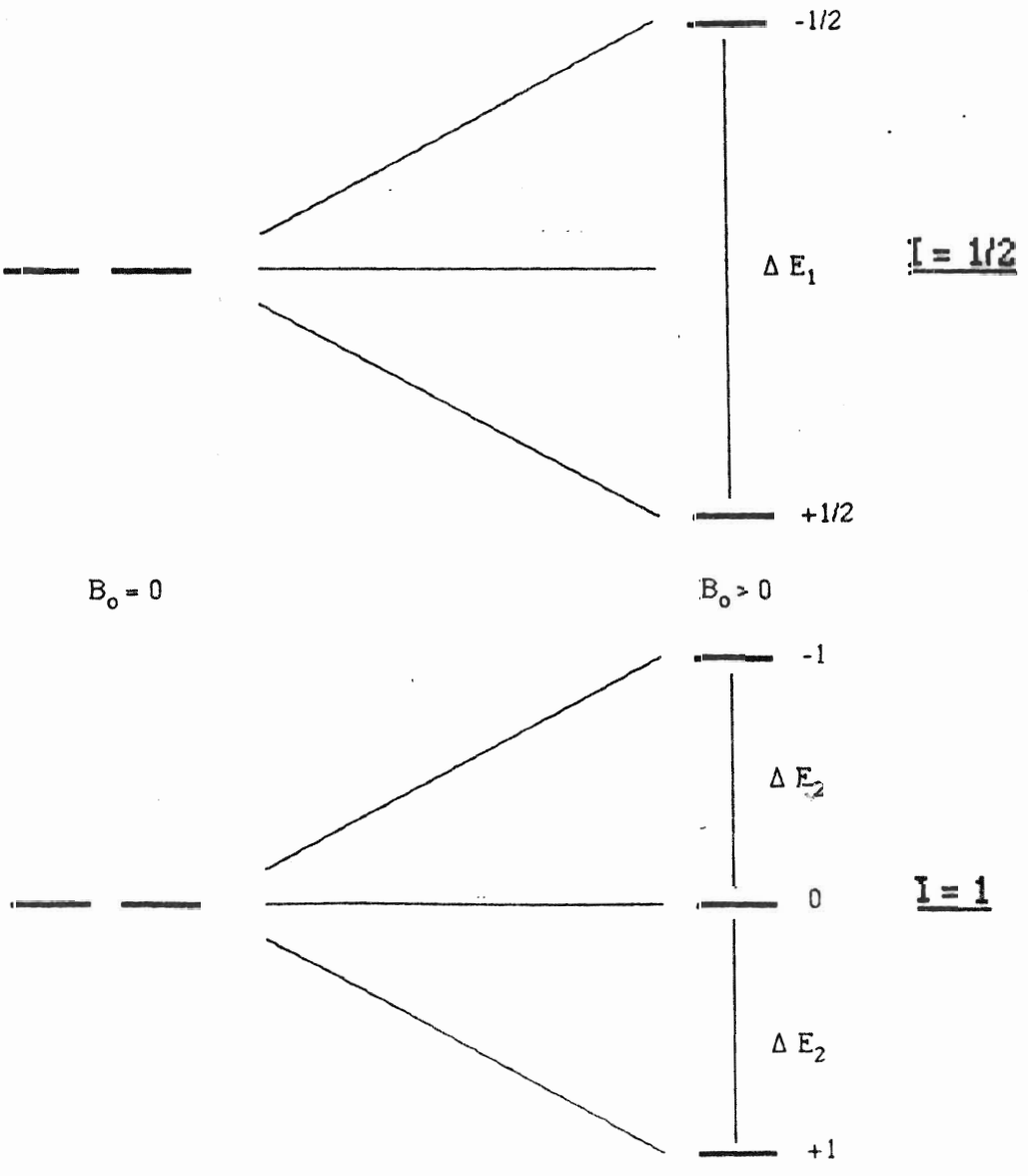

with: ν = frequency of absorption

γ = gyromagnetic ratio of nucleus

Bo = external magnetic field

$$\gamma = \frac{2\pi\mu}{hI} \qquad 2$$

with: μ = magnetic moment

h = Planck's constant

I = spin quantum number

The absorption frequency corresponds to the precessional (Larmor) frequency of the nucleus.

The precise frequency of absorption depends on the local electronic environment of the nucleus; moving electrons in a magnetic field generate their own weak magnetic field which opposes the main external field. The small differences in the absorption frequency arising from the local field are known to the chemist in more familiar terms as the chemical shift.

When using Fourier transform-NMR, data is collected as a signal which decays as some function (often exponential) of time. The frequency information of interest is contained as periodic oscillations within the envelope of the free induction decay (FID). Although not a trivial process, the frequency(ies) of absorption can be obtained mathematically by performing the following Fourier transform integration:

$$F(\nu) = \int_{t=0}^{\infty} f(t)\, e^{-2\pi i t \nu} dt \qquad 3$$

with: F(ν) = frequency function

f(t) = time function

In practice, the calculation is streamlined by using the fast Fourier transform (FFT) employing the Cooley-Tukey algorithm, and approximating integrals with summations.

(B) Historical Outline of NMR

Nuclear magnetic resonance (NMR) spectroscopy is a powerful analytical tool with applications to many of the natural sciences and medicine. The method can trace its origins back to the experiments and theoretical musings of physicists in the 1920's.[1]

NMR remained the domain of the physicist well into the 1950's; chemists and others had to wait until commercially viable instrumentation was introduced before they could reap the rewards proffered by studies of the radio frequency (RF) absorption spectra of nuclear systems.

The early commercial NMR spectrometers operated on the continuous wave (CW) principle, whereby the RF absorption spectrum is obtained by systematically and constantly varying the magnetic field which is bathing the sample, while applying a constant RF field.[1,2] This was fine for organic chemists who needed a tool to assist them in characterizing their compounds based on the chemical shifts and splitting patterns in the NMR spectra of nuclei with large gyromagnetic ratios and a high natural abundance. For those working with crystalline, ionic or polymeric compounds, or for that matter any solid substance, NMR was not even considered as an analytical tool. The breakthroughs which have made NMR spectroscopy the formidable

technique which it is, came from several independent sources. The first, the idea of pulsed NMR, had been around as long as CW NMR, but remained securely in the hands of physicists. Pulsed NMR involves applying an RF pulse of finite duration, containing all potential absorption frequencies, to a sample which is shrouded in a (hopefully) homogeneous, invariant magnetic field.[1] Information about the absorption frequencies as well as the dephasing of the transverse magnetization is stored as a free induction decay (FID). The information obtained relating to the transverse or spin-spin relaxation in the system defines the relaxation rate T_2^{-1}.[1]

The second factor which led to the blooming of modern NMR spectroscopy is the introduction of silicon-chip technology into computers dedicated to NMR-data processing. Solid state computers have the combination of memory and speed which permit Fourier transformation (FT) of an FID into a useful frequency domain signal, in an acceptable period of time (the fast Fourier transform (FFT) employing the Cooley-Tukey algorithm has further increased efficiency).[1]

Finally, the union of FT-NMR with superconductivity technology has resulted in the state-of-the-art spectrometer whose heart is cryogenic superconducting magnet with a field strength which may exceed 11.7T.

The FT-NMR spectrometer with high resolution probe is second to none when it comes to peak separation in the spectra of liquid samples. Disappointment awaits the researcher who attempts to use this setup for a solid sample however, for what

emerges is an enormously broad, featureless hump.

The breakthrough came when it was realized that it is possible to suppress many of the dipolar interactions which result in peak broadening in solids. By physically spinning the sample at several kHz such that the axis of rotation is inclined at the "magic angle" to the lines of force of the spectrometer's main magnetic field, the Hamiltonian operators governing like-dipole-dipole (spin diffusion), chemical shift anisotropy (CSA), and first order quadrupolar interactions become tiny or vanish. In our minerals, only the dipole-dipole mechanisms are important, although a small CSA contribution to peak broadening is likely. The probability expressions which contain the operators in multiplicative sequence also become tiny or vanish, and the interactions are thus greatly reduced or vanish.[3]

$$W_{ij} = \left(\frac{\gamma^2 h^2}{r_{ij}^3}\right)(1-3\cos^2\theta)$$

with: W_{ij} = dipole-dipole operator

γ = nuclear gyromagnetic ratio

h = Planck's constant

r_{ij} = interparticle separation

θ = angle of spin axis with respect to magnetic field

The field of magic angle spinning (MAS) NMR of solids is quite extensive, and many excellent references exist for those who want to delve into this subject in greater depth.[4,5]

(C) NMR of Silicates

The NMR of silicates was a natural outgrowth of MAS NMR

techniques, the field expanding rapidly once the technology which makes it possible was in place.

Lippma and co-workers did much of the pioneering work on the NMR of silicates.[6] They found that the chemical shift for a given ^{29}Si site in a given mineral can be predicted to fall within a certain range based upon how many Si-O-Si bonds are present. Although these ranges overlap considerably, the correlation is still significant: for no Si-O-Si bonds (SiO_4 tetrahedra not cross-linked at all--designated Q^0, orthosilicates or nesosilicates) the resonance comes between -60 and -83ppm, for 1 Si-O-Si bond per Si atom (Q^1 or sorosilicates) the range is -68 to -85ppm and -87 to -97ppm, for Q^2 (inosilicates) sites the range is -75 to -95ppm, for Q^3 (phyllosilicates) sites the range is -91 to -98ppm and for Q^4 (SiO_2 polymorphs) sites the range is -107 to -120ppm.[6] It should be noted that the above mentioned ranges don't include silicates containing 4-coordinate Al or Be. Thus we see that the trend is for the chemical shift to be found farther upfield the greater the degree of silicate condensation.

(D) Magic Angle Spinning NMR

NMR experiments using liquids have several advantages; motional averaging yields very narrow linewidths, making high resolution work possible. The speed at which the NMR tube spins about an axis orthogonal to the main field is typically 15-20 Hz, fast enough to effectively average out magnetic field inhomogeneities.

If one attempts to run the NMR spectrum of a solid under the same conditions which are used for liquids, the result

normally is an extremely broad, featureless hump. Not surprisingly, this result discouraged active research in the field of solids' NMR.

However, a few intrepid pioneers persevered, making progress on both the theoretical and the experimental-technological fronts. What finally emerged was one of the milestones in the evolution of experimental NMR: magic angle spinning (MAS) technology. MAS involves physically spinning the solid sample of interest at speeds varying from 2-10+ kHz, about an axis which is inclined at 54.74° to the main magnetic field of the spectrometer.[5]

The sample may be pulverized into a fine dust, exist as one lump, or be present in some form between the two extremes. In most cases, a fine dust free of clumps is desired in order to ensure a uniform distribution of mass within the spinner and hence rotation free from precession or wobble. This also increases the chances that all possible crystal orientations are equally represented. The angle is chosen as 54.74° in order to minimize the value of the above-mentioned Hamiltonians, although due to the nature of the equipment involved, one is unable to be sure in practice how close to this value one really is.

(E) Spin-Lattice Relaxation

Spin lattice relaxation involves attaining a Boltzmann equilibrium for the population of nuclear spins under consideration, after having perturbed the equilibrium or having initially placed the sample into a magnetic field.

As we are interested specifically in ^{29}Si , we will consider

the example of an I=1/2 nucleus. We are faced with 2 spin states, the lower energy alpha state with a component parallel to the main field, and the higher energy beta state, with a component antiparallel to the main field.

The Boltzmann distribution for a nuclear population placed into a magnetic field is:[7]

$$\frac{N_\alpha}{N_\beta} = e^{\frac{\Delta E}{kT}} \qquad 5$$

When the exponent is very small, we have the following approximation:

$$\frac{N_\alpha}{N_\beta} = 1 + \frac{\Delta E}{kT} \qquad 6$$

with: k = Boltzmann constant

T = absolute temperature

$\Delta E = 2\mu Bo$ = the energy difference between the alpha and beta spin states

Bo = main external field

μ = component of magnetic moment of nucleus aligned with Bo

In the case of the inversion recovery experiment, we follow relaxation behaviour from an initial condition of:

$$\frac{N_\beta}{N_\alpha} = 1 + \frac{\Delta E}{kT} \qquad 7$$

For saturation recovery, the experiment begins with:

$$N_\alpha = N_\beta \qquad (8)$$

The pulse sequence for inversion recovery, the pulse sequence for saturation recovery, and a typical inversion recovery stack plot are illustrated in Figures 2, 3, and 4 respectively.

(F) Why Study Spin-Lattice Relaxation in Silicates?

Although it may not always be obvious, spin-lattice relaxation affects everyone who does NMR work. Spin-lattice relaxation governs the rate at which nuclear populations reach equilibrium in the spectrometer's main field, and hence the frequency at which it is feasible to pulse.

For those doing quantitative NMR work, a thorough understanding of spin-lattice relaxation times is a prerequisite for reliable results.

The connection with silicates is quantitative work done to determine the relative amounts of the various components in ceramics and minerals. For a meaningful comparison of peak areas, one must be sure that 98%-99% of the nuclei in every different chemical site are contributing to their respective signals. Since spin-lattice relaxation in the above-mentioned systems is usually due to interactions with paramagnetic impurities, we chose to study synthetic minerals with similar properties. As a result, we hoped to be able to explain spin-lattice relaxation in compact silicate structures in such a way that those doing quantitative work could benefit from our discoveries.

FIGURE 2

The Inversion Recovery Pulse Sequence for Spin-Lattice Relaxation Time Measurement

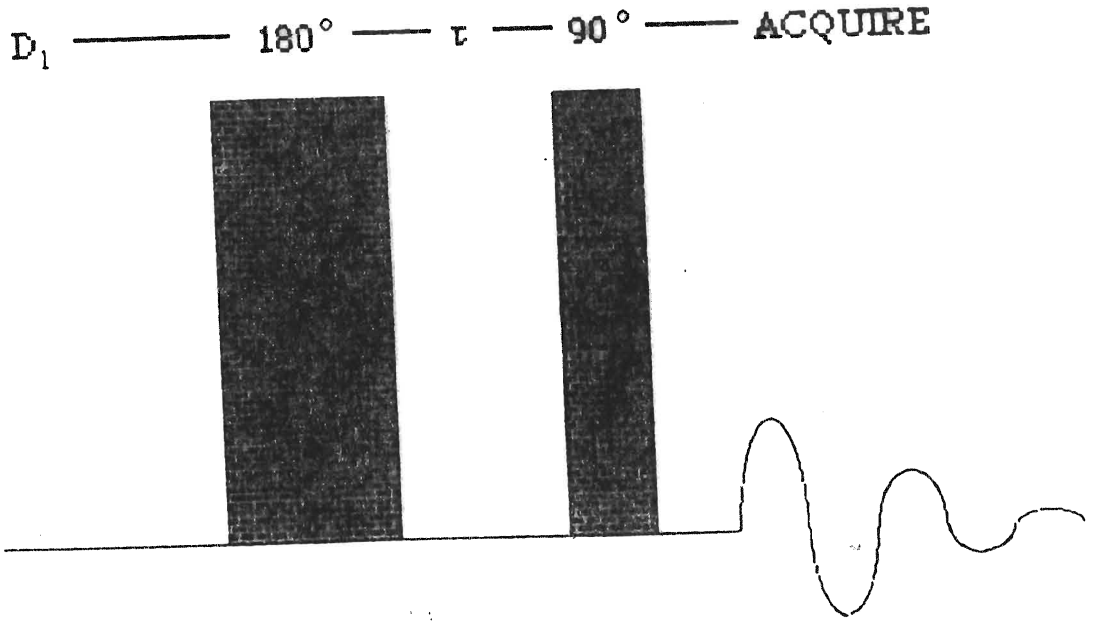

FIGURE 3

The Saturation Recovery Pulse Sequence for Spin-Lattice Relaxation Time Measurement

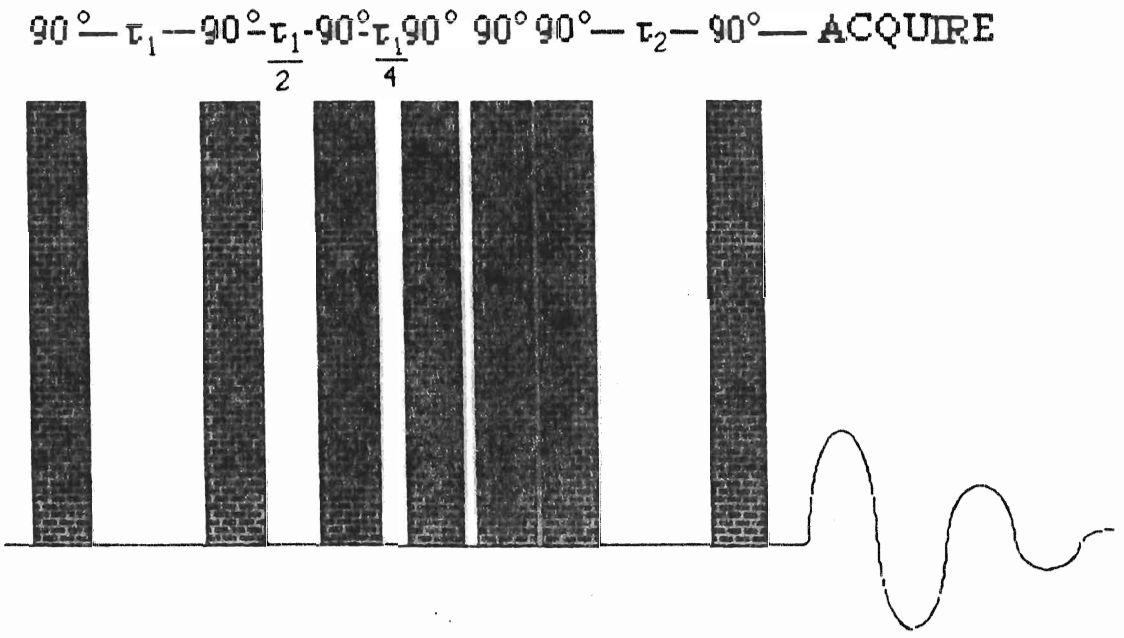

FIGURE 4

This is a typical inversion recovery stack plot. The mineral is a forsterite doped with 0.1% Cu(II); note that the spectrum contains one singlet.

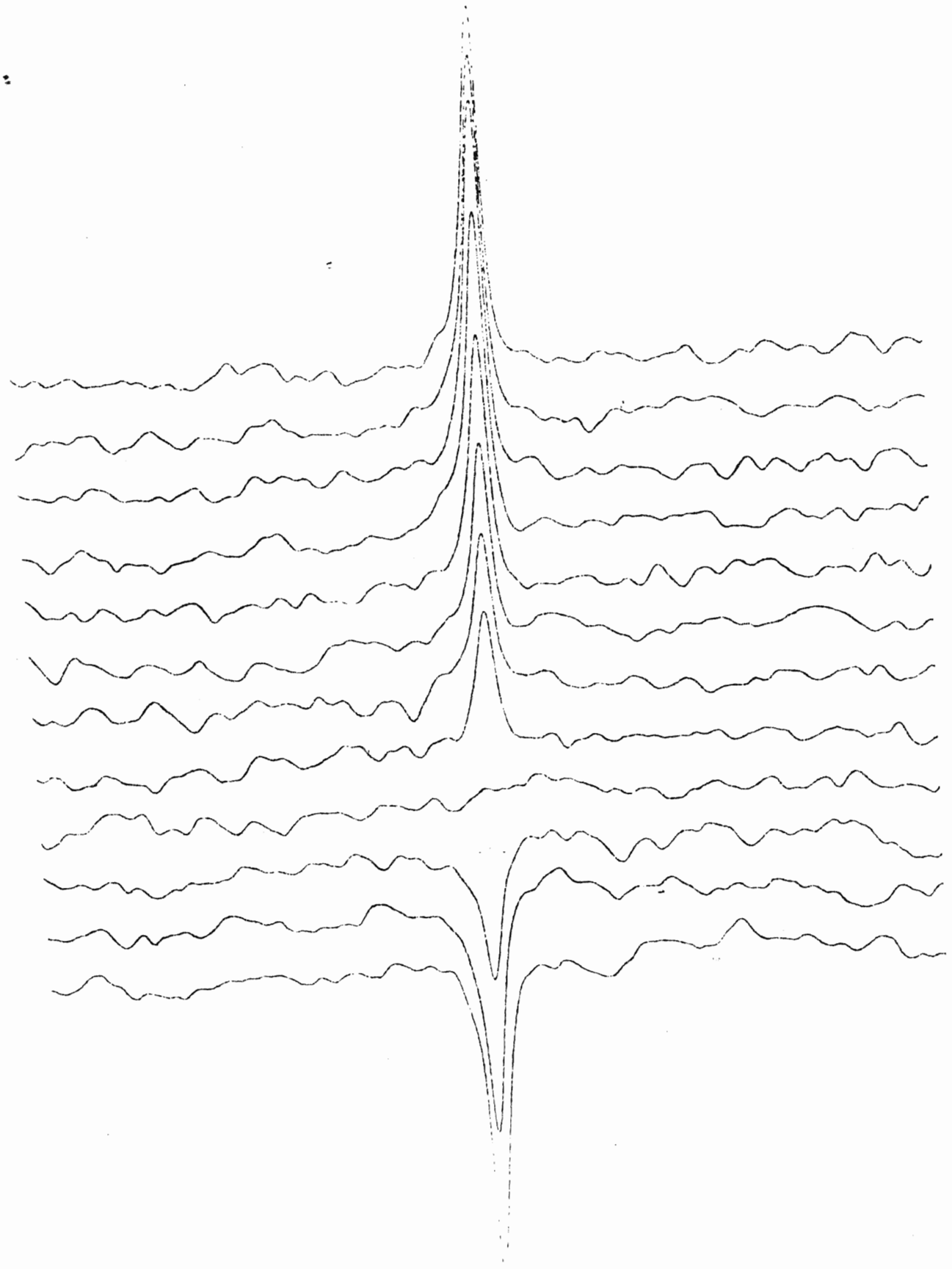

(G) Nonexponential Spin-Lattice Relaxation in MAS NMR

It is widely assumed that longitudinal nuclear magnetic relaxation follows an exponential rate law: $Y=\exp(-t/T_1)$, where Y is the normalized signal intensity, t is time, and T_1 is the spin-lattice relaxation time. This is not surprising, for even a cursory survey of advanced general texts[1] exposes the interested reader to the simple exponential expression containing T_1. Indeed, the software package loaded onto the dedicated computers in Bruker NMR systems performs a 3 parameter exponential regression when determining T_1's from spin-lattice relaxation data.[8]

The stretched-exponential: $Y=\exp[-(t/T_n)^n]$, with n being the stretch parameter and T_n being the relaxation time (spin-lattice relaxation time in the context of this work), is by no means uncommon, and appears not only in NMR relaxation but in mechanical relaxation, dispersive transport phenomena, and dielectric relaxation.[9] A comparison of the exponential and stretched-exponential can be seen in Figure 5.

The earliest known appearance of the stretched-exponential in the literature was in 1864, and is attributed to Kohlrausch.[10] Kohlrausch was working with mechanical deformations. A brief general summary of the history of the stretched-exponential in the literature can be found in reference 11.

What concerns us is the literature background dealing specifically with stretched-exponential magnetic relaxation observed using NMR techniques.

Although not explicitly dealing with stretched-

FIGURE 5

This is a comparison of the exponential and 1/2 power stretched-exponential function, for equivalent relaxation times.

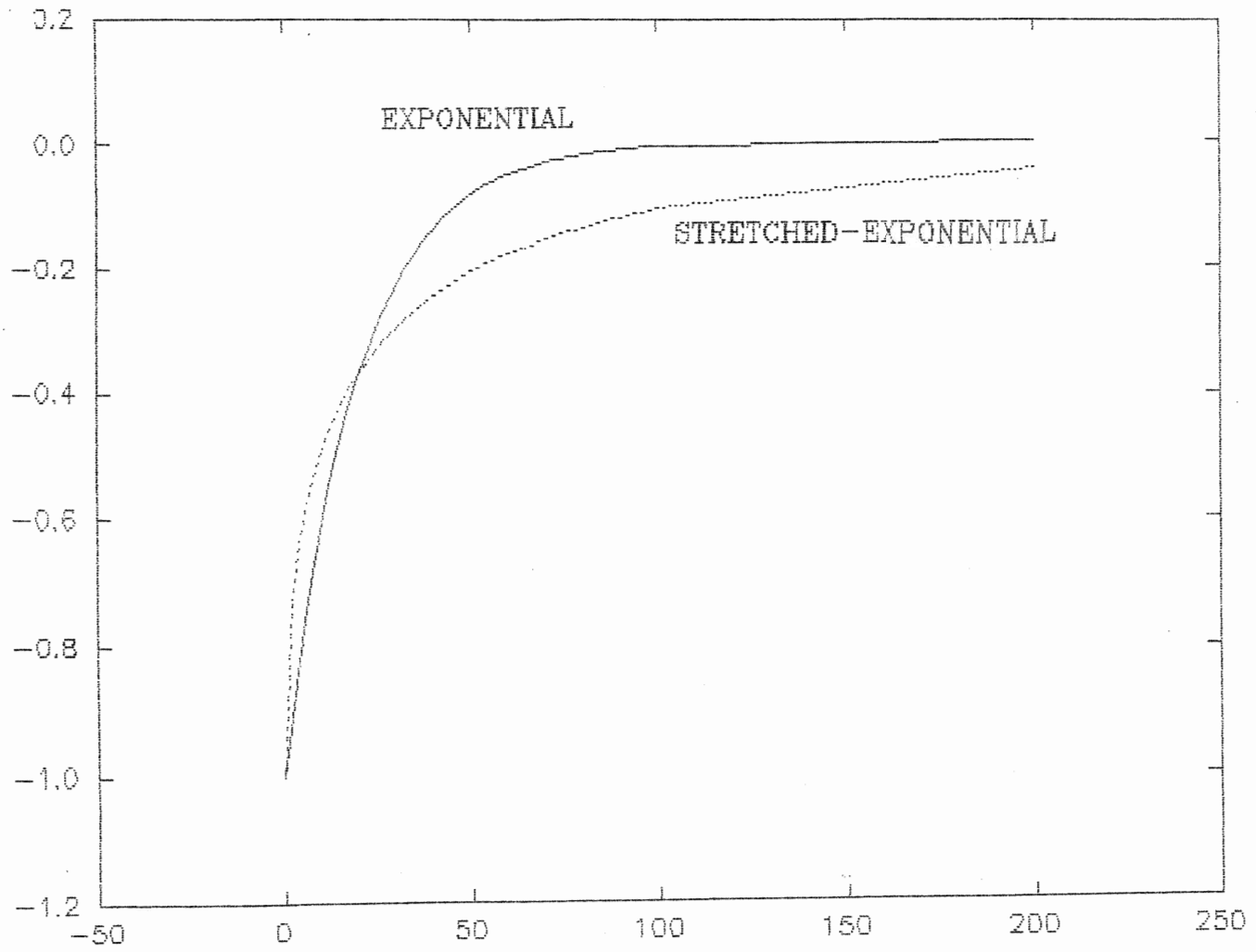

exponentials, but rather the 1/2-power with respect to time decay function which supersedes the exponential decay function in the absence of spin diffusion, Blumberg's paper about nuclear spin-lattice relaxation
in crystals containing randomly distributed paramagnetic ion impurities is the first major work in the field.[12] This highly mathematical and somewhat confusing work deals with our area of concern only in general terms, and hence is not all that useful. Tse and Hartmann performed spin-lattice relaxation MAS NMR experiments on CaF_2 doped with 0.06 mole percent Eu(III).[13] A study of the relaxation of the ^{19}F nuclear population in which spin diffusion has been suppressed yields the 1/2-power stretched-exponential rate law: $Y=\exp[-(t/T_{0.5})^{0.5}]$.[13]

Maiti and McGarvey also contributed to this field; their experimental material is solid $Fe(phen)_2$ $(N^{13}CS)_2$.[14] ^{13}C spin-lattice relaxation times were determined for one ligand site which was progressively enriched with this nucleus. At lower enrichment levels, they found that the system obeyed a 1/2-power stretched-exponential rate law. When ^{13}C enrichment reached 90 percent at the relevant site, relaxation was neither exponential nor 1/2-power stretched-exponential (they don't say what it was); this deviation was attributed to the onset of spin diffusion.[14]

While our own work was in progress Thangaraj and Ganapathy performed a ^{29}Si relaxation study on Na-Y and ZSM-5 zeolites.[15] They found that spin-lattice relaxation proceeded as a 1/2-power stretched-exponential function of time. They found spin-spin

relaxation to be exponential. The Shlesinger and Klafter paper dealing with nonexponential relaxation attempts to explain the underlying factors which lead to the observed functions.[11] It proposes three mechanisms which can
lead to stretched-exponential decay with respect to time: "direct transfer on a fractal," "fractal time defect diffusion," or relaxational processes which are constrained by the innate hierarchical structure of the material. All of these mechanisms lead to a common scenario: a hierarchy of relaxation times with a sufficiently broad distribution to assure a nonintegral exponent for time.[11] This process typically operates along parallel pathways (driven by a product of relaxation probability functions arising from many paramagnetic centres) but can be a 2-body interaction.

A recent paper dealt with the ^{29}Si spin-lattice relaxation behaviour of synthetic network silicates doped with low concentrations of paramagnetic ions.[16] The theoretical foundation of their work is Blumberg's paper.[12] Their experimental data fits power law regression curves.[16]

Exponential spin-lattice relaxation has been reported for many silicates (zeolites and phyllosilicates)[17-19] (although it was only stated explicitly in reference 19, the others apparently assuming that this was the case), and for dilute ^{13}C systems.[20] In the case of the silicates, there is an extremely efficient dipole-dipole relaxation mechanism in operation, dipolar electron relaxation, which arises from molecular oxygen diffusing through the framework (in the case of zeolites) or

paramagnetic cations moving through the interlayer water as a result of Brownian motions (in the case of the phyllosilicates).[17-19,21]

In the case of natural abundance ^{13}C in a single crystal of type-IIb semiconducting diamond, the relaxation times are extremely long (3-4 hours). Spin-lattice relaxation occurs via 2 different mechanisms according to the authors: (i) interactions between nuclei and fixed paramagnetic impurities, and (ii) the movement of mobile holes in the valence band.[20]

(H) Spin-Lattice Relaxation Mechanisms in Network and Ionic Solids

The observed spin-lattice relaxation rate is a sum of relaxation rates arising from all possible longitudinal relaxation mechanisms:[1]

$$T_{1obs.}^{-1} = \sum_{i=1}^{k} T_{1i}^{-1} \qquad 9$$

or,

$$T_{nobs.}^{-1} = \sum_{j=1}^{q} T_{nj}^{-1} \qquad 10$$

In liquids, molecular motions play a predominant role in spin-lattice relaxation. However, in low temperature network solids, atomic motions are restricted to constrained vibrations.

(1) Electron-Nuclear Dipole Relaxation

One of the most efficient of all spin-lattice relaxation mechanisms arises from the magnetic dipolar interaction of unpaired electrons with nuclei. The effectiveness of this

mechanism is due almost exclusively to the formidable magnetic moment of the electron: 3 magnitudes or greater than those of nuclei.[1] The process involves a relaxational nuclear spin flip without a corresponding electron spin flip; the magnetic fluctuations occurring at the nuclear Larmor frequency arise from motions of the unpaired electron within the orbital which it occupies.

The relaxation rate due to electron-nuclear dipole interaction is, neglecting the angular dependence, as follows:[3]

$$\frac{1}{T_{1e}} = \frac{\left[\frac{2}{5}\gamma_S^2\gamma_I^2\left(\frac{h}{2\pi}\right)^2 S(S+1)\frac{\tau}{1+\omega_I\tau^2}\right]}{r^6} \qquad \textbf{11}$$

with: r = mean electron-nuclear separation

γ = gyromagnetic ratio, I = nuclear, S = electronic

h = Planck's constant

S = electronic quantum spin number

τ = longitudinal electronic relaxation time

ω = nuclear Larmor frequency

Theoretically, for relaxation by paramagnetic impurities in solids, the longitudinal relaxation time should be inversely proportional to the concentration of paramagnetic impurities. In the case of limited spin diffusion:[3]

$$T_1^{-1} = 4\pi D\rho\,[M^{2+}] \qquad \textbf{12}$$

with: ρ = pseudopotential radius ($B_e = B_o$)

B_e = locally generated magnetic field

D = spin diffusion constant, $D=Wx^2$

x = internuclear separation

W = mutual spin flip probability

As has been shown earlier, the magnetic moment is determined by the gyromagnetic ratio. Also of interest is the sixth-power distance dependency of the spin-lattice relaxation time, making this predominantly a local mechanism.

There is a region close to the paramagnetic impurity where $B_c=B_o$; nuclei falling within this critical radius do not contribute to the spectral line. Rather, they are markedly broadened and shifted out of the frequency envelope of the exciting RF pulse.

There is also a scalar electron-nuclear dipole mechanism, which can arise if the orbital wavefunction of the unpaired electron is nonzero at the relevant nucleus.[3] This is a mutual spin flip process. As it usually occurs in paramagnetic molecules or ions, we discount the dominance of this mechanism in orthosilicates, even though orbital overlap is still possible.

(2) Spin Diffusion

Nuclei of the same type, in similar magnetic environments, can undergo a mutual, magnetic-dipole spin flip interaction. The equilibration of nuclear spin state populations which results from many such interactions is known as spin diffusion. It is a relaxation mechanism, which allows paramagnetic impurities in an ionic/network solid to relax nuclei through a pathway other

than direct electronic-nuclear dipolar interaction. Thus, if we have the conditions illustrated initially in Figure 6 (A), we find that all of the excited nuclei are eventually relaxed, even though electron-nuclear dipolar relaxation only takes place between the paramagnetic centre and the nearest neighbour ^{29}Si nucleus. The first relaxational event occurs at the nearest neighbour nucleus in (B); as the relaxation mechanism is exhibits a probability inversely proportional to the sixth power of the interparticle separation, relaxation takes place here due to probabilistic factors. In situation (C), there is a mutual magnetic moment spin flip between adjacent nuclei. Again, this process is directly proportional to the interparticle separation. The same process which occured in step (C) occurs again in step (D) and (E). At a much later time, the second relaxational event occurs (F). Once again, the nucleus relaxed by the paramagnectic centre is the one closest to it. Steps (G) and (H) are characterized by mutual nuclear spin flips as in step (C). The third relaxational event occurs at step (I). Step (J) is the equivalent of step (C). The final relaxational event occurs in step (K). The dotted arrows represent spin diffusion propagating out through the lattice, or, put another way, the efficient reduction of the spin temperature gradient. The nuclei are able to effectively communicate their spin temperature with one another: in other words the spin temperature in the system equilibrates rapidly between relaxational events. Figure 6 illustrates the conditions which give rise to exponential spin-lattice relaxation. Figure 7

illustrates the same system relaxing in the absence of spin diffusion. Here, we have poor equilibration of spin temperature, and thus a distance dependent hierarchy of nuclear spin-lattice relaxation times. Figure 7 illustrates the conditions which give rise to stretched-exponential spin-lattice relaxation. Step (A) is the equivalent of step (A) in Figure 6, the companion figure. We find a single paramagnetic impurity and a population of four excited nuclei. The first relaxational event occurs in step (B). The inverse sixth power dependence of the electron-nuclear dipolar relaxation mechanism assures that the nucleus nearest to the paramagnetic center is by far the most likely to be relaxed first. Step (C) illustrates the second relaxational event. Probability factors again dominate, causing relaxation to occur at the paramagnetic centre's next nearest neighbour nucleus. Steps (D) and (E) are a continuation of this trend. Both Figures 6 and 7 are highly schematic, and don't take the Boltzmann equilibrium into account as this would muddle the effects which are being illustrated.

(3) Quadrupolar Relaxation

Nuclei with I>1/2 possess a quadrupole moment which can interact with the electric field gradients associated with the local atomic electron cloud.[1]

$$\frac{1}{T_{1Q}} = \frac{3}{40}\left(\frac{2I+3}{I^2(2I-1)}\right)\left(1+\frac{\eta^2}{3}\right)\left(\frac{e^2qQ}{h}\right)\tau_c$$

with: T_{1Q} = component of spin-lattice relaxation time arising due to quadrupolar interactions

η = quadrupole asymmetry parameter

FIGURE 6

Relaxation with Rapid Spin Diffusion

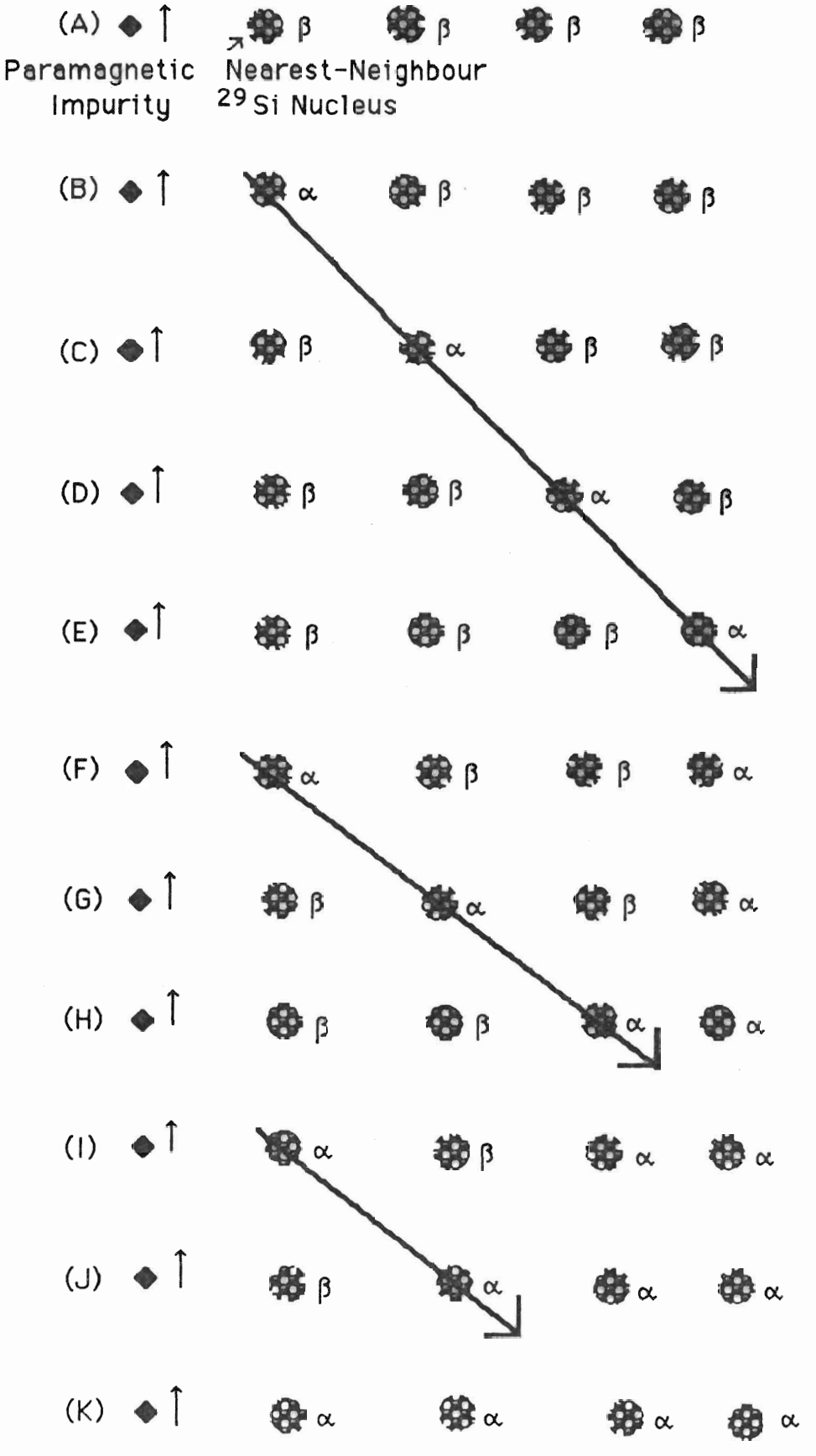

FIGURE 7

Relaxation with Limited Spin Diffusion

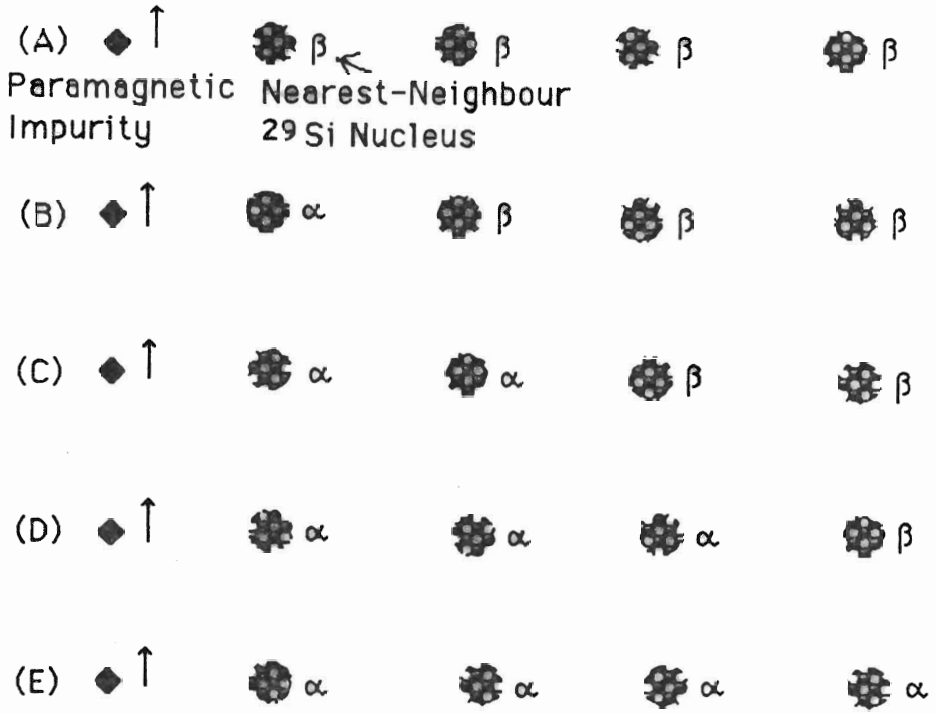

q = electric field gradient at nucleus

e = charge on electron

eQ = charge on nucleus

This mechanism can be ruled out as a viable relaxation agent in our studies because ^{29}Si has I=1/2.

(I) Spin-Spin Relaxation Mechanisms in Network and Ionic Solids

Spin-spin relaxation is the process of magnetization dephasing which occurs in the plane perpendicular to the main field.

(1) Paramagnetic-Nuclear Dipolar

Interaction of the electronic magnetic moment associated with the paramagnetic impurity with the nuclear magnetic dipole contributes to the dephasing of x-y magnetization in solids.[7] As with T_1,

$$T_2 \propto \frac{1}{[M^{2+}]} \qquad (14)$$

In our paramagnetics-doped orthosilicate systems, this is likely the dominant spin-spin relaxation mechanism, as has been shown by previous studies which indicate a correlation between peak width at half height and the concentration of the paramagnetic dopant.[22]

(2) B_o Inhomogeneities

If the main magnetic field of the spectrometer (B_o) is not perfectly homogeneous (and it never is), then the field gradient will dephase the magnetization. This is not an intrinsic spin-spin relaxation mechanism and is always distinguished from the naturally occurring phenomena. It also makes spin-spin

relaxation times (T_2's) relatively meaningless unless the spectrometer effect can be corrected for. Thus, we have in general:

$$\frac{1}{T_{2obs.}} = \frac{1}{T_{2B_o}} + \sum_{i=1}^{x} \frac{1}{T_{2i}} \qquad 15$$

For solids, $T_2 < T_1$ in all cases.[23]

(J) Structure of Orthosilicates

Silicates exhibit myriad structures; in addition to the silicon-oxygen framework large numbers of cations and anions of various sizes and charges can be incorporated into the lattice. The orthosilicates which we are interested in are comparatively simple, containing as they do one or two types of metal cations in appreciable quantities and SiO_4^{4-} anions.

Forsterite (Mg_2SiO_4) forms orthorhombic crystals.[24] The structure (see Figure 8[24,25]) can be thought of as an ionic crystal composed of SiO_4^{4-} and Mg^{2+}, or, alternatively as a covalent network. Silicon is tetrahedrally coordinated with respect to oxygen, while Mg^{2+} and the dopant cations populate the two different types of octahedral sites formed by the oxygen network. Put another way, the oxygen atoms form a distorted hexagonally close-packed lattice, with the silicon atoms occupying the tetrahedral voids and the magnesium and transition metal (which readily replace magnesium if of a similar size) atoms occupying the octahedral voids.[24]

Willemite (Zn_2SiO_4) forms hexagonal crystals.[26] The structure (see Figure 9[26,27]) is similar to phenacite (Be_2SiO_4), though somewhat distorted due to the fact that the Zn-O mean

separation is greater than the Si-O mean separation.[27] The lattice is composed of tetrahedra of oxygen atom which are joined at the corners. Zinc and silicon atoms occupy the tetrahedral voids in a ratio of 2:1. In one direction, the tetrahedra appear to cluster around parallel C_3 axes such that the oxygen atom through which the axis passes is contained within an isosceles triangle formed by 2 Zn atoms and 1 Si atom.[26]

(K) Sol-Gel Synthesis of Orthosilicates

Sol-gel methods involve the formation of solid silicates from precursor solutions. One big advantage which sol-gel techniques have over conventional synthetic methods is that they are a low-temperature procedure. This saves on energy expenditures and requires less costly equipment: even when a gel must be fired in order to effect recrystallization, the temperature required is much lower than if one were to attempt the procedure beginning with a mechanical mixture of the required oxides. Since sol-gel processes are in general quite slow, it is possible to pour the precursor solution into a mold where the silicate then polymerizes. When very intricate or complex forms are required, the advantages over attempting to shape heated material are obvious.

The sol-gel procedure for synthesizing orthosilicates can be described, in its simplest form as making minerals by condensing organo-silicates and metal cations:

Dissolution:

$Si(OEt)_4$ (l)+ $2Mg(NO_3)_2$ + excess 95% EtOH ----> ethanolic solution

FIGURE 8

Here is the idealized forsterite structure, after Bragg and Brown (1926).[24]

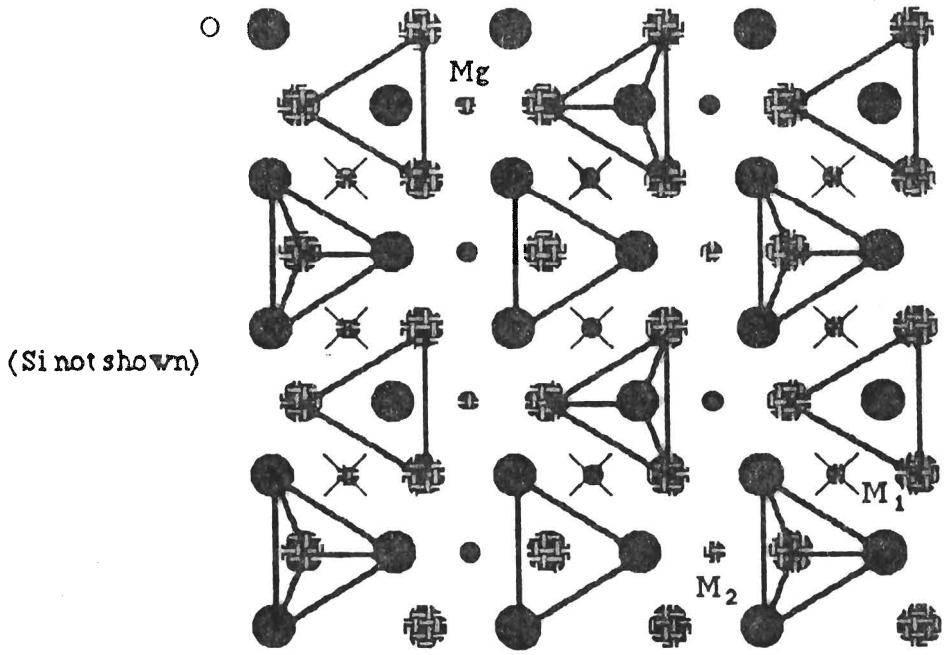

This figure illustrates structure of olivine $(Mg,Fe)_2SiO_4$, after Bragg and West.[25]

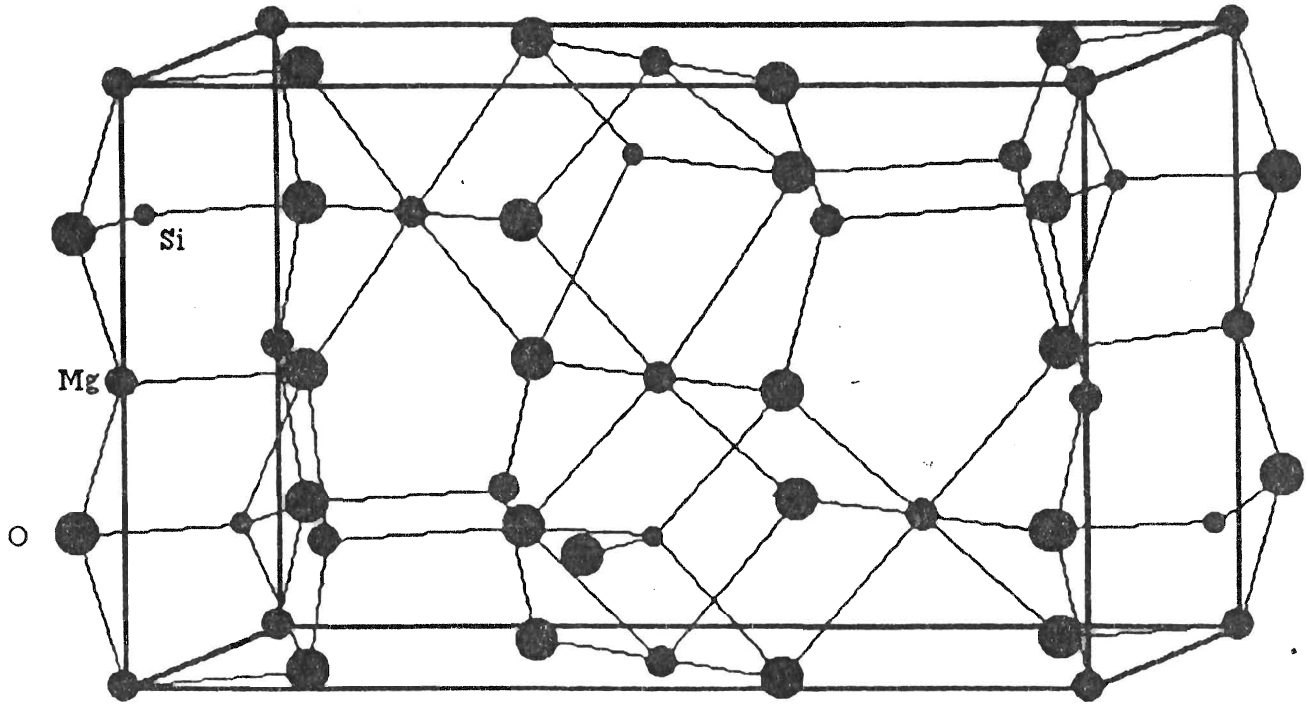

FIGURE 9

The structure of willemite; the corners of the tetrahedra contain oxygen atoms, after Hang and coworkers.[26]

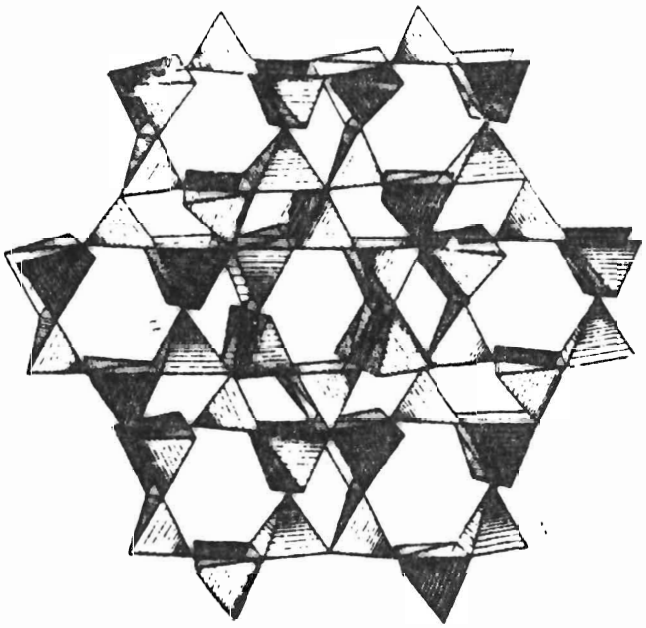

The structure of phenacite, a willemite analog, is shown here. The small atoms are silicon, the large oxygen, after Bragg and Zachariasen.[27]

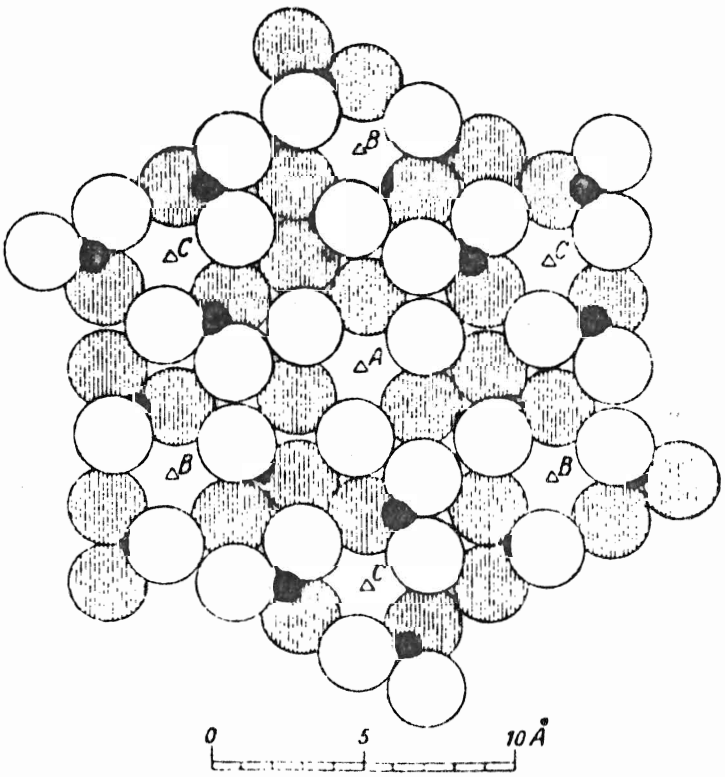

Hydrolysis and Condensation:

$Si(OEt)_4 + H_2O$ ----> $(OEt)_3Si\text{-}OH + EtOH$

$(OEt)_3Si\text{-}OH + (OEt)_3Si\text{-}OH$ ----> $(OEt)_3Si\text{-}O\text{-}Si(OEt)_3 + H_2O$

Hydrolysis and condensation continue until a SiO_2 polymorph is present.

Solvent Removal:

Heat at 80° C in a water bath and later at 110° C in a drying oven.

Nitrate Removal:

At 400° C in a tube furnace under inert atmosphere:

$2Mg(NO_3)_2$ ----> $2MgO + 4NO_2 + O_2$

Forsterite Crystallization:

At 1100° C in a tube furnace under inert atmosphere:

$2MgO + SiO_2$ ----> Mg_2SiO_4

These formulae typify the general nitrate decomposition and forsterite crystallization reactions; the actual reactions may be more complex (see reference 30, page 777). The primary application of this technique is in the ceramics and related industries, where polymerization of the organo-silicate is of primary interest. Consequently, much of the developmental work in this area relates to ceramics, literature being available on the subject.[28,29,30] The references contained within chapter 3 of reference 29 represent a fairly complete documentation of the history of the sol-gel method.

(L) X-Ray Diffraction Powder Pattern Spectroscopy

There are three types of x-ray spectroscopy, absorption, fluorescence and diffraction. X-rays are produced by electrons striking the anode in a vacuum tube.[31] The transfer of electronic kinetic energy in one or more steps creates a continuum of x-ray emission within

the allowed energy range. The continuum will contain several absorption lines corresponding to quantum transitions within the electronic shell of the atoms making up the anode. X-rays so generated are employed in one of the above-mentioned three areas.

X-ray diffraction is only effective for crystalline materials; it is the repetitive nature of the structure which makes distinct absorption or emission peaks possible. Amorphous materials can absorb x-rays, but it will be over a continuous range, and hence the method is useless for these substances.

X-ray absorption and fluorescence are used in qualitative and to some extent quantitative elemental analysis.[31] For identification of crystalline material, single crystal or powder, x-ray diffraction methods are employed.

X-ray diffraction powder pattern employs a powder camera and monochromatic x-ray source.[31] The camera is cylindrical, with the sample at a point along the central axis and the film along the wall. The diffraction of the x-ray beam from the sample generates cones of x-radiation which are recorded on the film.[31] In more modern instruments, photodiodes and remote recorders are used in place of film. Although the calculations won't be detailed here,
the camera dimensions and diffraction angles can be used to determine the crystal plane separations in the sample.[31]

(M) Direct Current Plasma Arc Spectroscopy

DCP is a high temperature method of emission spectroscopy, used in qualitative and quantitative elemental analysis.

Volatilization of the sample in a low voltage, high current discharge rapidly heats it to between 4000 and 6000K, temperatures at which the atoms are exhibiting thermal emission.[31] The light from the plasma is focused into the spectrometer, onto a photodetector. For a given element, one wavelength will be examined (usually the strongest emission line). For quantitative work, known standards and blanks are also required.

EXPERIMENTAL

(A) NMR Measurements

(1) NMR Instrumentation

NMR experiments were run on Bruker AC-200 and AM-500 spectrometers. Both machines employ superconducting cryomagnets, the field for the AC-200 being 4.7 T, and that of the AM-500 being 11.7 T. As well, both spectrometers are interfaced to dedicated Bruker Aspect-3000 computers.

The AC-200 uses a home-made MAS probe of the Andrew-Beams type, employing Delrin (polyformaldehyde) spinners.[4] The MAS probe employed by the AM-500 system is a Doty design, employing precision-machined parts and two air flows, bearing and spinning, for extra stability at high speeds.

A spinning speed of 3 kHz was typically used with the AC-200. Spinning speeds of 7-8 kHz were the norm for the AM-500 system, although a few inversion recovery spin-lattice relaxation measurements were made at 11.7T and 3 kHz in order to check for field strength and spinning speed induced variations.

Spectra, except where otherwise noted, have a line broadening of 250 Hz, and are polynomial baseline-corrected where necessary.

For ^{29}Si, a 90° pulse typically corresponds to 25.1 and 5.0 to 8.0 microseconds on the AC-200 and AM-500 respectively.

(2) MAS NMR Pulse Experiments

(i) Inversion Recovery

Most of our spin-lattice relaxation times were measured

using the inversion recovery method. The basic pulse sequence is:[8]

$$---(-180^{o}-\tau-90^{o}-ACQUIRE-D_1-)_x---$$

with: τ = variable delay

D_1 = fixed delay

The data were fitted to a 3-parameter exponential regression function on the Aspect-3000:

$$F(t)=A3+A2*\exp(-\frac{t}{T_1}) \qquad \textbf{16}$$

where F(t) is the peak height (intensity) measured by the Aspect-3000 computer, and t is equivalent to the relevant tau. This results in the pseudo T_1's (spin-lattice relaxation times generated when the poorly fitting exponential regression is used) quoted in our Results section. These results were tabulated for comparison with the actual relaxation times to show the pitfalls of using the wrong regression function.

The 4-parameter stretched-exponential regression required to properly describe the inversion recovery data was run with the Sigma-Plot program on an IBM 286 or 386.

$$F(t)=A3+A2*\exp[-(\frac{t}{T_n})^{n}] \qquad \textbf{17}$$

In order to test the validity of the Sigma-Plot results, a stretched-exponential regression was run for an inversion recovery data set which should have been exponential (proton 4 on indole in D_2O solution). We found n=0.995+/-0.01; a good fit to the expected result of n=1.000, so we accepted the accuracy of this program.

(ii) Saturation Recovery

The Bruker software was modified in order to remove an unwanted delay related to decoupler power switching: the delay made it impossible to get tau < 2ms. The basic modified pulse sequence is:[8]

$$---(-[90^{o}-D_2-90^{o}-\frac{D_2}{2}-90^{o}-\frac{D_2}{4}-...-1ms-90^{o}-]-\tau-90^{o}-ACQUIRE-)_x---$$

When compared with the inversion recovery pulse sequence, the average power output for the saturation recovery pulse sequence is quite high, due to the fact that there is a comb of 10 to 20 90° pulses and saturation recovery does not use the long fixed delay inherent in inversion recovery. Soon after running the saturation recovery experiment, we noticed that one of the capacitors had been damaged. While we cannot claim beyond a shadow of a doubt that the saturation recovery experiment caused the damage, we chose not to try again and risk destroying a hard to replace part, such as a tuning capacitor.

(iii) CPMG-T_2 Experiments

Spin-spin relaxation behaviour was examined for 3 forsterites and 3 willemites, each doped with 2.5% Co(II), Ni(II), or Cu(II).

The Carr-Purcell-Meiboom-Gill experiment uses the following basic pulse sequence:[1,8]

$$---[D_1-90^{o}--(-D_2-180^{o}_y-D_2-)_a--ACQUIRE-]_b---$$

(B) Sol-Gel Synthesis and Thermal Recrystallization

Our synthesis method is based on that of Kazakos and co-workers,[32] who synthesized forsterite, but willemite has been

made by a similar method.[33] The metal(II) nitrate-hydrates are weighed out in the proper proportions for a given sample and then dissolved, with vigorous stirring, in 95% ethanol.

TEOS (tetraethylorthosilicate) is propipetted into the ethanolic solution, again with stirring, this time to promote initial homogeneity.

Ethanol is used as the solvent instead of distilled water because TEOS and water are immiscible.

The beaker containing the reaction mixture is Teflon, as early experiments with Pyrex glass vessels served to exhibit the remarkable adhesive powers of the wet gel. Frosting of the Pyrex beakers observed after removing the gel with $HCl_{(aq)}$ indicates a reaction between the glass beaker and solution.

Solvent removal prior to gelation is enhanced by using a water bath at 60°C to 80°C.

After gelation, the sample is dried in air at 110° C for at least 16 hours. High temperature recrystallization is carried out in a quartz tube furnace under argon or nitrogen. Heating for typically 2 hours at 400° C drives off the remaining volatiles, including the nitrate ion decomposition products as nitrogen oxides. The samples are then fired at 1100° C for at least 18 hours to facilitate ion migration, hopefully generating a random or near-random distribution of paramagnetic impurities. Mineral structures are verified using ^{29}Si NMR chemical shifts for all samples and x-ray diffraction (XRD) powder pattern spectroscopy for some. The correlation between sol-gel sample names and compositions can be found in Table 1.

TABLE 1: Sol-Gel Sample Name-Composition Correlation

Mol % M^{2+} (x+/-0.5X)	Mg_2SiO_4				Zn_2SiO_4			
	Undoped	Co^{2+}	Ni^{2+}	Cu^{2+}	Undoped	Co^{2+}	Ni^{2+}	Cu^{2+}
0.0	F4				W1			
0.1		F12	F13	F11		W9	W10	
0.2								W8
0.35				F17				
0.45		F21						
0.75				F18				
1.0		F5	F3	F6		W3	W4	W2
1.9				F19				
2.5		F15	F16	F14		W13	W11	W12
4.3				F20				
5.0		F9	F10	F8		W6	W7	W5
7.5						3P31C		
10.0			3P31B					
15.0				MCu6*				
20.0								3P31A

Note: * is not a sol gel sample; it was formed as a precipitate from aqueous solution by M. Seifried

(C) X-Ray Diffraction Powder Pattern Spectroscopy

XRD studies of crystals utilize the diffraction angles and crystal-plane separations to deduce the structure.[31] For those who don't have complete crystals or are just interested in mineral identification, the XRD powder pattern provides a unique fingerprint.[34] As the XRD powder patterns of tens of thousands of compounds are known,identification is usually possible using the literature.[31] Computer searches of this data-base are by far the most efficient, but manual searches are still viable. For a manual search, one begins with the most intense peak, then the second most intense peak, etc., (based on their D values), progressively narrowing down the choices. A match of the 8 most intense peaks with the literature spectrum is taken to be positive identification.

The computer search using the aforementioned software package operates in 3 stages: data input, a coarse search for the 100 closest matches, and finally a line by line precision characterization to identify the mineral(s) present.

Our XRD spectra were run and assigned by computer at the University of Manitoba. The work was carried out using a PW1710 spectrometer with a dedicated IBM PC computer system which employs the Fein-Marquart microPDSM-Micro Powder Diffraction Search Match program.

X-rays were produced by a Cu-anode x-ray tube; a single wavelength was selected using a curved graphite monochromator.[35] The scan range was 10° to 100° 2-theta, at a rate of 0.03° 2-theta per second.[35]

(D) DCP Spectroscopy

In order to verify the dopant concentrations in our synthetic orthosilicates, we selected 3 willemite samples for direct current plasma-arc (DCP) spectroscopic analysis.

The instrument used is a Beckman Spectra Scan V, user time on which was generously provided by Professor Ian Brindle.

The preparation method involves fusing the orthosilicates with lithium metaborate ($LiBO_2$) at 1100°+ C for at least one half hour in a 95% platinum, 5% gold crucible, inside a muffle furnace. The molten sample is then poured into 1% nitric acid, where upon it solidifies and shatters. Heating and ultrasound are needed to dissolve the samples.

The sample is then allowed to flow into the plasma arc. The volatilized sample enters the observation region and the intensity at the relevant emission wavelength is observed.[31] For cobalt the wavelength is 340.50 nm, for nickel 305.08 nm, and for copper 324.75 nm. Two standard solutions containing known amounts of the metal ions are needed for calibration, as is a blank solution.

RESULTS

(A) T_1, T_n, n Measurements

The core of our orthosilicate work involved the investigation of spin-lattice relaxation behaviour. The regression results are presented in Tables 2-6. It is obvious that considerably fewer than half of the n values agree with the predicted 1/2 value (ie. $0.4 < n < 0.6$). In the case of lower dopant concentrations this anomalous result is almost certainly due to too few experimental points or a too-short fixed delay which has the effect of compressing the curve with respect to time. Observing and describing this effect is central to our work. Using too few points, or weighting the data in favour of shorter times may introduce errors, but we have not studied these effects. Using a fixed delay in the inversion recovery experiment which is too short has the net effect of making the experimentor believe that 99% recovery has occurred, when in fact it has not. Thus, when the data is normalized, all of the points indicate apparently more complete relaxation than has actually occurred. The effect of this systematic error is to artificially increase the value of n when the 4-parameter stretched-exponential regression is performed.

However, there are genuine cases of deviation from 1/2-power at higher dopant concentrations. In cases where the fixed delay is more than adequate, there are 5 such examples; willemites with 2.5%, 5%, and 7.5% Co(II), and 20% Cu(II), and a forsterite with 15% Cu(II). The value of n proffered by Sigma-Plot for the spin-lattice relaxation in these cases is:

Table A

Sample	B_o (T)	n	Spinning Speed (kHz)	
willemite with 2.5% Co^{2+}		0	4.7	0.84
		3	4.7	0.77
		0	11.7	0.87
		3	11.7	0.95
		8	11.7	0.69
willemite with 5% Co^{2+}		3	4.7	0.84
		8	11.7	0.83
willemite with 7.5% Co^{2+}		3	4.7	0.82
willemite with 20% Cu^{2+}		3	4.7	0.71
forsterite with 2.5% Cu^{2+}		3	4.7	0.48-0.49
		3	11.7	0.57
		7	11.7	0.47
forsterite with 15% Cu^{2+}		3	4.7	0.83
		6	11.7	0.77

Due to the varying quality of data and different conditions, it is difficult to draw a comparison between work done at 4.7 T and work done at 11.7 T. However, based on the data for forsterite with 2.5% Cu^{2+} and willemite with 2.5% Co^{2+}, we tentatively conclude that spin-lattice relaxation is more efficient at lower magnetic field strengths (4.7 T), other things being equal. The data is not conclusive, probably due to large experimental errors, when it comes to the effect of spinning speed on spin-lattice relaxation times.

It has been predicted that the relaxation time should be inversely proportional to the concentration of a given paramagnetic impurity.[12] Although we see some pairs of values which obey this relation, it is not generally followed for an entire series.

However, a rough correlation is seen for the Co(II)-doped forsterites, Ni(II)-doped forsterites, Co(II)-doped willemites, and Cu(II)-doped willemites.

In most cases, T_1 and T_n differ by much less than a factor of 2. In some cases, there are no differences at all when experimental error is taken into account. The exceptions are invariably for very long relaxation times, when the fixed delay is on the order of a magnitude too short. Under such conditions, the exponential is a poorer fit than normal, and T_1 appears much too short.

We used a saturation recovery experiment to verify our inversion recovery data for one sample. In comparing the saturation recovery data to the inversion recovery results, found in Table 2, we find than n agrees within 3.5%, T_n agrees within 14.8%, and T_1 agrees within 12.5% of the inversion recovery value.

The following formula was used to calculate the above percentages:

$$\% = \frac{|SATREC - INVREC|}{INVREC} x100\%$$

TABLE 2: Forsterite Spin-Lattice Relaxation Data at 4.7T (3kHz and Nonspinning)

Composition	T_n (s)	n	No. of Data Points	D_1 (s)
Undoped	$7.6X10^3$+	0.51	12	4000
Co^{2+} 0.1%	149	0.50	8	500
1%	23.6	0.69	12	100
1%	42.1	0.62	10	2500
2.5%	8.30	0.68	12	25
5%	2.97	0.79	12	20
5%	3.44	0.79	8	150
Ni^{2+} 0.1%	1.56	0.66	12	10
1%	0.190	0.57	12	1
2.5%	0.115	0.57	12	20
SATREC2.5%	0.132	0.59	12	---
5%	0.030	0.59	8	1
10%	0.011	0.71	15	0.5
Cu^{2+} 0.1%	90.7	0.51	12	3000
1%	23.0	0.47	8	500
2.5%	0.449	0.49	15	50
2.5%	0.469	0.48	15	50
5%	0.083	0.70	8	2
nospin5%	0.073	0.69	8	2
15%	0.024	0.83	20	1

Note: SATREC indicates saturation recovery pulse sequence.

TABLE 3: Willemite Spin-Lattice Relaxation Data at 4.7T (3kHz and Nonspinning)

Composition	T_n (s)	n	No. of Points	D_1 (s)
Undoped	$3.1X10^3$+	set to 0.50	10	3600
Co^{2+} 0.1%	9.49	0.62	8	100
1%	0.732	0.67	12	10
2.5%	0.181	0.77	15	9.3
nospin2.5%	0.192	0.84	10	9.3
5%	0.072	0.84	15	10
7.5%	0.071	0.82	15	5
Ni^{2+} 0.1%	$2.3X10^3$+	0.46	8	3600
2.5%	242	0.74	8	2500
Cu^{2+} 0.2%	448	0.62	8	4000
1%	155	0.58	6	1000
nospin1%	94	0.83	7	1000
2.5%	33.8	0.57	12	500
5%	16.4	0.63	15	300
20%	2.75	0.71	11	110

TABLE 4: Forsterite and Willemite Spin-Lattice Relaxation Data Compared at 4.7T (0 and 3 kHz) and 11.7T (0, 3, and 6-8 kHz)

Composition	T_n(s)	n	No. of Points	D_1(s)	H_o(T)	Spin(kHz)
Forsterite						
5% Ni^{2+}	0.03	0.83	8	1	4.7	3
5% Ni^{2+}	0.117	0.58	16	2.5	11.7	8
2.5% Cu^{2+}	0.449 -0.469	0.49 -0.48	15	50	4.7	3
2.5% Cu^{2+}	1.02	0.57	15	18	11.7	3
2.5% Cu^{2+}	0.618	0.47	20	25	11.7	7
15% Cu^{2+}	0.024	0.83	20	1	4.7	3
15% Cu^{2+}	0.028	0.77	20	1	11.7	6
Willemite						
2.5% Co^{2+}	0.192	0.84	10	9.3	4.7	0
2.5% Co^{2+}	0.181	0.77	15	9.3	4.7	3
2.5% Co^{2+}	0.243	0.87	12	9.3	11.7	0
2.5% Co^{2+}	0.333	0.95	13	9.3	11.7	3
2.5% Co^{2+}	0.330	0.69	16	20	11.7	8
5% Co^{2+}	0.072	0.84	15	10	4.7	3
5%Co^{2+}	0.121	0.83	20	3	11.7	8

TABLE 5: Forsterite Pseudo-T_1's and T_n's Compared at 4.7T

Composition	Pseudo-T_1 (s)	T_n (s)
Undoped	1213+	7631+
Co^{2+} 0.1%	89.5	149
1%	45.0	42.1
2.5%	6.00	8.30
5%	3.52	3.44
Ni^{2+} 0.1%	1.46	1.56
1%	0.150	0.190
2.5%	0.112	0.115
SATREC 2.5%	0.126	0.132
5%	0.071	0.030
10%	0.011	0.011
Cu^{2+} 0.1%	99.3	90.7
0.45%	4.99	5.25
1.0%	19.8	23.0
2.5%	0.469-0.497	0.449-0.469
4.3%	0.175	0.215
5%	0.088	0.083
nospin 5%	0.079	0.073
15%	0.024	0.024

TABLE 6: Willemite Pseudo-T_1's and T_n's Compared at 4.7T

Composition	Pseudo-T_1 (s)	T_n (s)
Undoped	1089+	$3.1X10^3$+
Co^{2+} 0.1%	16.2	9.49
1%	0.763	0.732
2.5%	0.182	0.181
5%	0.072	0.072
7.5%	0.071	0.071
Ni^{2+} 0.1%	505+	$2.3X10^3$+
2.5%	234	242
Cu^{2+} 0.2%	329	448
1%	128	155
nospin1%	100	94
2.5%	33.2	33.8
nospin2.5%	0.183	0.192
5%	15.7	16.4
20%	2.76	2.75

(B) Spin-Lattice Relaxation Behaviour in Naturally Occuring Pyroxenes

In addition to our study of synthetic orthosilicates, a limited spin-lattice relaxation investigation was conducted for natural pyroxenes (diopsides--$Ca(Mg,Fe^{2+})Si_2O_6$ and omphacites--$(Ca,Na)(Mg,Fe^{2+},Fe^{3+},Al)Si_2O_6$). The iron content had already been determined using Mossbauer spectroscopy.[36] The ^{29}Si MAS NMR spectra had a line broadening of 250 Hz applied, leaving only 1 apparent peak in the spectrum; this was done due to time constraints. The spin-lattice relaxation behaviour is stretched-exponential. Data is presented in Table 7.

It will be noted that the fixed delays are not long enough. This is because this work was carried out before we realized that there was a bias toward n = 0.5. Consequently, these results are tentative and some the work must be repeated.

(C) T_2 Measurements

As an adjunct to our spin-lattice relaxation work, we have studied the spin-spin relaxation behaviour of some of our orthosilicate samples.

We found that the transverse magnetization decay exhibited large oscillations in intensity (see Figure 9A). As a result, it isn't possible to make a definitive statement with respect to the exponential or stretched-exponential nature of the overall decay.

Values of T_2 incorporate a relaxation component derived from magnetic field inhomogeneities; thus the numbers obtained have no value in absolute terms, but their relative values are of some interest. The shape of the decay curve is what provoked

TABLE 7: Spin-Lattice Relaxation Data for Natural Pyroxenes at 4.7T and 3 kHz

Sample	No. of Fe^{2+} Atoms per 6 O Atoms	No. of Fe^{3+} Atoms per 6 O Atoms	T_1(s)	T_n(s)	n	D_1(s)
BLW065 omphacite	0.04	0.01	0.210	0.233	0.67	unknown
BLW067 omphacite	0.08	0.06	0.0133	0.0201	0.62	0.20
BLW014 diopside	0.086	<0.01	0.0772	0.0818	0.71	1.00
BLW017 diopside	0.012	<0.001	0.678	0.690	0.66	15.00
BLW109 diopside	0.07	<0.003	0.249	0.436	0.62	2.50

FIGURE 9A

Sample CPMG Data

```
MINIMUM T1-    .050 .110 MAXIMUM T1= 20.000 1

T1 NOT WITHIN CURRENT LIMITS, CHANGE LIMITS:
MINIMUM T1=    .110 .001 MAXIMUM T1-  1.000
```

CURSOR	FREQ	PPM	T2	STD DEV	
987	-2840.617	-71.4427	.05607	.135193	
TAU	CURSOR	FREQ	PPM	INTEGRAL	INTENSITY
.0000	985	-2816.203	-70.829	111.630	82.974
.0001	985	-2816.203	-70.829	72.756	51.815
.0010	984	-2803.996	-70.522	164.667	89.085
.0030	984	-2803.996	-70.522	48.945	36.603
.0050	984	-2803.996	-70.522	155.696	90.354
.0070	985	-2816.203	-70.829	81.171	47.587
.0100	984	2803.996	-70.522	97.638	67.159
.0200	985	-2816.203	-70.829	76.040	43.695
.0300	984	-2803.996	-70.522	47.866	35.231
.0400	984	-2803.996	-70.522	31.366	22.555
.0499	985	-2816.203	-70.829	74.260	48.280
.0599	984	-2803.996	-70.522	32.393	27.049
.0700	985	-2816.203	-70.829	41.858	27.779
.0799	985	-2816.203	-70.829	23.509	19.142
.0899	985	-2816.203	-70.829	16.672	13.116
.0999	985	-2816.203	-70.829	29.127	20.258
.1199	985	-2816.203	-70.829	15.906	11.440
.1400	985	-2816.203	-70.829	9.399	8.639
.1599	986	-2828.410	-71.136	10.879	8.614
.1799	985	-2816.203	-70.829	12.957	8.217
.1999	986	-2828.410	-71.136	7.926	6.624
.2999	987	-2840.617	-71.443	2.110	2.341

A1= .056070 A2= .703959 A3= .049798

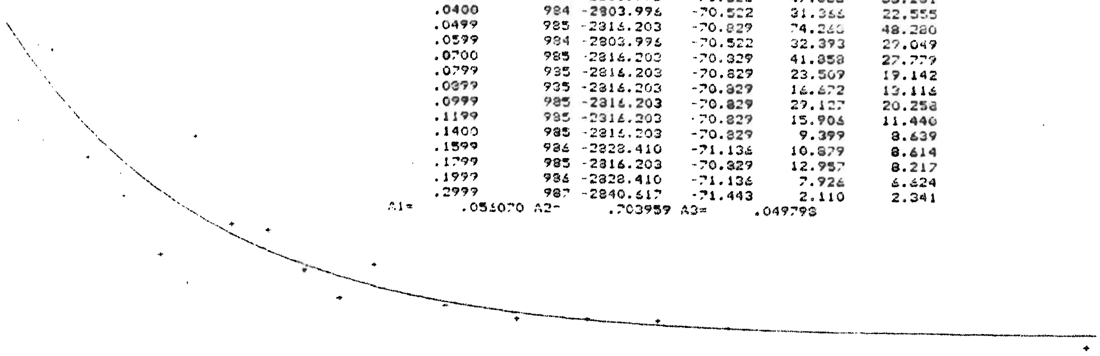

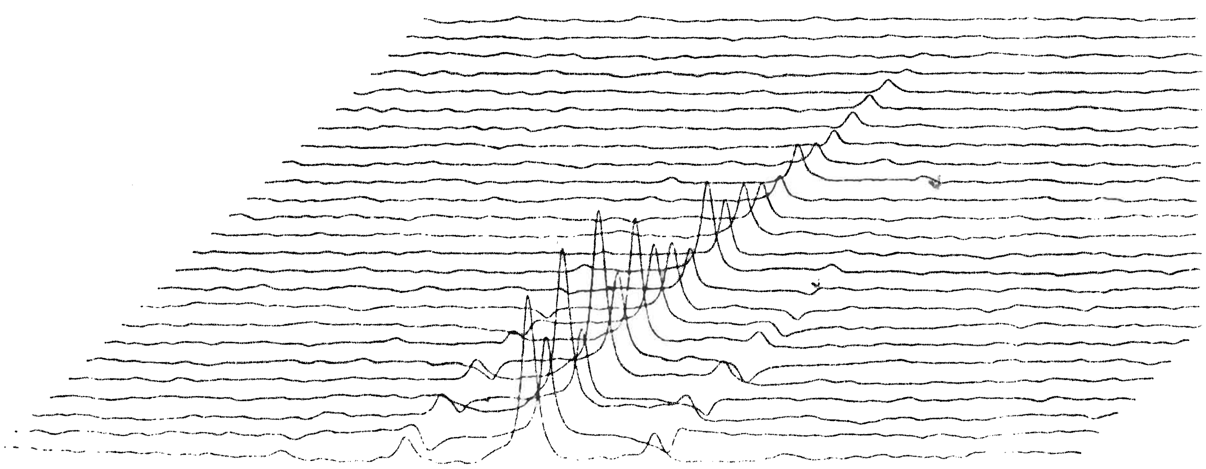

PAHN ECHO-T [illegible]

our interest in performing these experiments.

(D) XRD Analysis

We obtained XRD analyses of 9 of our synthetic orthosilicates. The results are documented in Table 8. For the 8 sol-gel samples, it is obvious that the synthesis and firing yielded the expected compound. Small amounts of MgO/ZnO or enstatite indicate a slight excess of metal nitrate or orthosilicate respectively, in the initial solution.

The forsterite synthesized from sodium orthosilicate and magnesium chloride by M.Seifried was analyzed because we had done some work on these compounds and in fact used 1 measurement for this work. The presence of large quantities of NaCl confirms our fear that there is a viable mechanism for dopant metal ion loss ($CuCl_2$ melts at 620° C and boils at 993° C, $CoCl_2$ melts at 724° C and boils at 1049° C, and $NiCl_2$ melts at 1001° C but sublimes at 973° C)[37] at our firing temperature of 1100° C. Thus we avoided this method of synthesis, and even the 1 value we quote (for forsterite with 15% Cu(II)) should be greeted with caution, as the Cu(II) concentration is uncertain.

(E) DCP Analysis

The DCP work performed on 6 samples was done to determine the error in the dopant concentrations which we quoted. The results of this work can be found in Table 9.

TABLE 8: XRD Results for Selected Forsterites and Willemites

Sample	Major Minerals	Minor Minerals < 10%
RLF050 (Undoped)	forsterite,	halite (NaCl)
MCu6 (15% Cu^{2+})	forsterite	enstatite ($MgSiO_3$)
F8 (5% Cu^{2+})	forsterite	enstatite
F9 (5% Co^{2+})	forsterite	periclase (MgO)
F10 (5% Ni^{2+})	forsterite	periclase
W5 (5% Cu^{2+})	willemite	
W8 (0.2% Cu^{2+})	willemite	
W9 (0.1% Co^{2+})	willemite	zincite(ZnO)
W10 (0.1% Ni^{2+})	willemite	
W11 (2.5% Ni^{2+})	willemite	zincite

TABLE 9: DCP Results for Selected Forsterites and Willemites

Sample	Expected Dopant	Measured Dopant
W2	0.99% Cu^{2+}	0.43% Cu^{2+}
W3	1.00% Co^{2+}	1.32% Co^{2+}
W4	1.01% Ni^{2+}	1.29% Ni^{2+}

DISCUSSION

(A) Characterization of Orthosilicates

Lippmaa and co-workers report one singlet in the ^{29}Si MAS NMR spectrum of synthetic forsterite at delta = -61.9 ppm with respect to tetramethylsilane.[6] Synthetic olivine with between 1 and 5 percent Fe(II), has a singlet at -62 ppm with respect to tetramethylsilane.[6] For undoped forsterite, we found one singlet at -61.6 ppm. To confirm the specific shift of willemite, we consulted the work of Seifried and Hartman, which involved an alternate synthetic method (provoking instantaneous and possibly chaotic precipitation from aqueous solution by exceeding the K_{sp}).[22] Good agreement was obtained between that study and this one; the willemite ^{29}Si spectrum in both cases contained one singlet, at -70.1 ppm in the Seifried work, and at -70.6 ppm in our work.

Most samples received only the "soft" treatment: the expected NMR chemical shift confirms the crystalline structure. As this is clearly risky, the "hard" method-XRD powder pattern analysis-was employed for a select number of samples. Only a limited number of samples were analyzed due to the considerable cost of the service; we do not have adequate machinery to do it here at Brock. Since all of the sol-gel samples were made via the same method, we did not anticipate random variations in crystal structure; if some of our samples are tested and prove without exception to be what we expected, then we infer that all of our samples are composed of the correct mineral. We believe that the great quantity of metal cations present is the primary factor inhibiting silicate

polymerization.

In all cases,the synthesis was a success. The appearance of minor phases, relatively rich in either magnesium/zinc or silicon is probably due to the precursor solution containing nonstoichiometric amounts of the starting materials.

The other analysis, again performed on only a select number of samples for the same reason stated above, is DCP spectroscopic measurement of transition metal content. This was done to verify that our samples contain the same amount of paramagnetic ions that we claim. Again, the data is tabulated in the Results section. As can be seen, we find that there is more nickel and cobalt and significantly less copper than expected. Since the blank solution containing undoped willemite prepared in the same way as the samples analyzed contains only traces of these metals, we are at a loss to explain the discrepancy. The relative lack of copper is possibly due to the reagent having absorbed excess water prior to use. While no obvious reason exists for enrichment in cobalt and nickel, the need to extrapolate rather than interpolate from the standards (due to calculation misunderstandings) introduces errors of an unknown magnitude.

(B) Fractal Dimension and Its Relevance to Paramagnetics-Doped Forsterite and Willemite

If there is a fractal (noninteger) dimension in these materials, it will arise because the distribution of paramagnetics is neither random nor ordered.[38] A fractal dimension occurs if the impurities are distributed randomly on

FIGURE 10

Potential Paramagnetic Ion Distributions

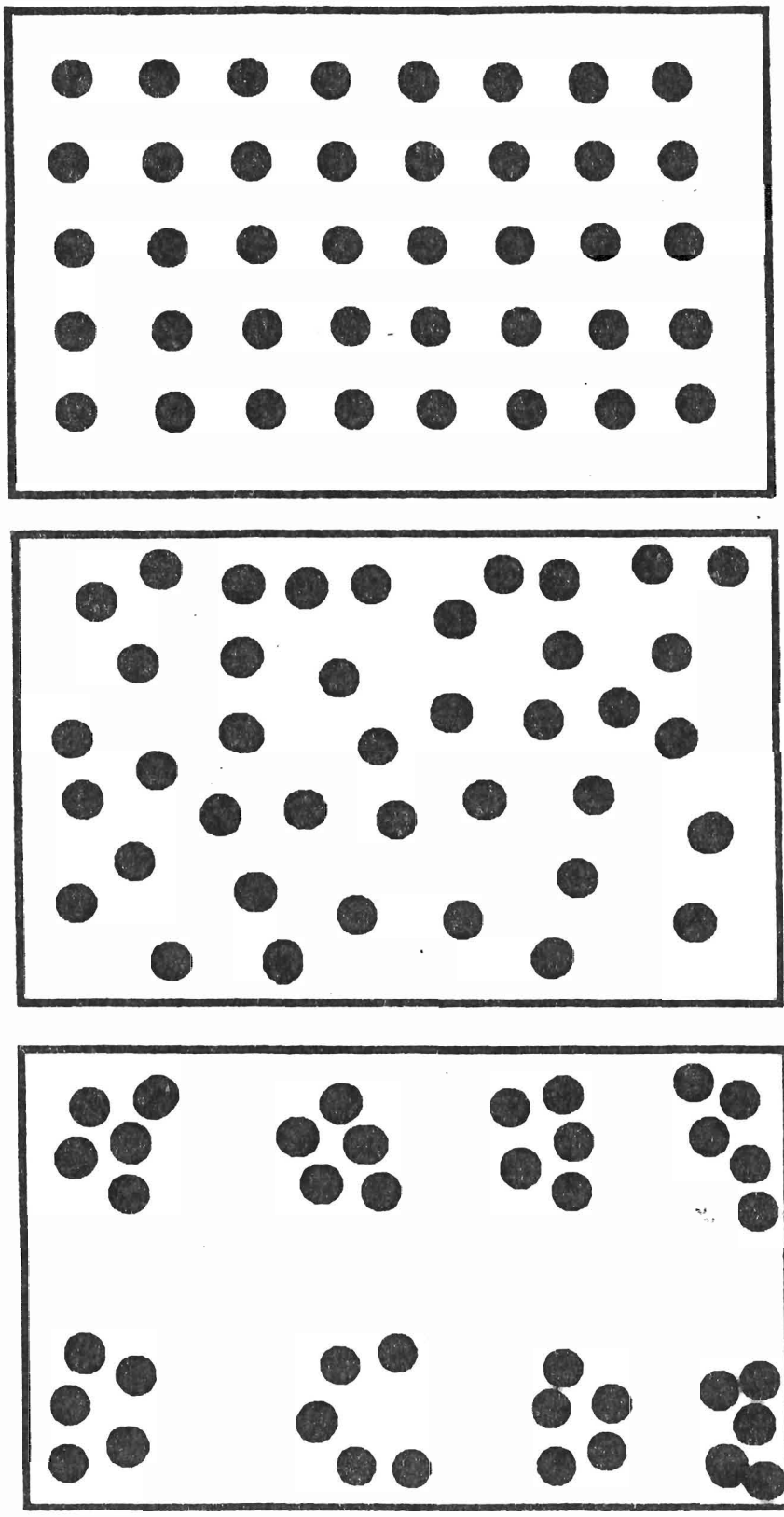

a limited local scale, but the concentration gradients are such that there is a clustering effect at larger scales (see Figure 10). Fractal dimensions may be nested, such that the large scale clustering is apparently random at that level but exhibits a recognizable order at an even larger scale.

Although we have no evidence one way or the other for the fractal dimension, it must be stated that either way, stretched-exponential decay is still viable. The only possible relevance is how it affects the shape of the stretched-exponential curve, specifically how it influences the value of the stretch parameter n.

(C) The Stretched-Exponential Explained

The outline which follows was adapted from Shlesinger and Klafter.[11]

Consider initially the magnetic dipolar interaction between an unpaired electron and a ^{29}Si nucleus in the beta spin state. The relaxational process, when it occurs, is a quantum event. The probability that the nucleus is still in the beta state at time t, is given by the following equation:

$$g(t,r) = \exp\left(-\frac{t}{T(r)}\right) \qquad \textbf{18}$$

where T(r) is the distance-dependent most-probable relaxation time.

Assuming a rigid lattice and the absence of a paramagnetic defect at the nucleus, we can now define an expression which encompasses the probability functions for all paramagnetic impurities as they relate to this nucleus:

$$G(t,r)=\prod_{i=1}^{x}\exp\left(-\frac{t}{T(r)_i}\right) \qquad 19$$

In order to take into account all possible paramagnetic sites in the lattice (corresponding to all octahedral voids in orthosilicates), we average over these sites, and introduce a probability of replacement parameter P to take the actual concentration into account:

$$F(t,r)=\prod_{i=1}^{x}\left[1-P+P\exp\left(-\frac{t}{T(r)_i}\right)\right] \qquad 20$$

If P << 1, as is the case when the concentration of the paramagnetics is low, then:

$$F(t,r)=\exp\left\{-P\sum_{i=1}^{x}\left[1-\exp\left(-\frac{t}{T(r)_i}\right)\right]\right\} \qquad 21$$

In order to transform the summation into an integration, we introduce the distance-averaging "site density function:"

$$S(r)=\sum_{i=1}^{x}b(r_o-r_i) \qquad 22$$

where r_o is the average paramagnetic-nuclear separation and b is the nuclear site function.

We now have:

$$F(t,r)=\exp\left\{-P\int_{r=0}^{\infty}b(r)\,dr\left[1-\exp\left(-\frac{t}{T(r)}\right)\right]\right\} \qquad 23$$

In the case of a dipole-dipole interaction, we have:

$$T(r) \propto r^{q} \qquad 24$$

When integration has taken place, the stretched-exponential appears:

$$F(t) = \exp\left[-\left(\frac{t}{T_n}\right)^{n}\right], \quad n = \frac{D}{q} \qquad 25$$

in D dimensions.

Since the dipolar interaction is in fact sixth-power, and we are working with a 3-dimensional structure, we find that:

$$n = \frac{3}{6} \rightarrow n = \frac{1}{2} \qquad 26$$

Hence we have:

$$F(t) = \exp\left[-\left(\frac{t}{T_{0.5}}\right)^{0.5}\right] \qquad 27$$

the half-power stretched-exponential decay function.

Two of our best data sets were fitted to an expression very similar to that in Devreux's paper;[16] as a result a power law dependency was ruled out for the spin-lattice relaxation behaviour of orthosilicates. These negative results are not presented but are easily reproducible.

In most cases our results conform to 1/2-power stretched-exponential decay, within experimental error. However, a few cases deviate such that $0.5 < n < 1$. The willemite doped with 5% Co(II) is the best example of this.

This may be due to a breakdown of the $P \ll 1$ condition, which thereby invalidates the subsequent approximation. Another possibility is that, since this theoretical treatment assumes random disorder (in this case a random distribution of

paramagnetic impurities), if we have a fractal distribution of paramagnetic centres at higher concentrations, a bias is being introduced for which there is no corresponding compensation.

As the stretched-exponential longitudinal magnetization relaxation in orthosilicates indicates, the rate of spin diffusion between ^{29}Si nuclei is negligible:

RATE (e-N dipolar relaxation) >> RATE (spin diffusion)

This may be due to the fact that ^{29}Si has a low natural abundance (4.7%).[39] There is, however, some experimental evidence which indicates that the ^{29}Si spin flip probability, W, may have a very small value.[40] This is highly suspect though, as recent MAS NMR study of synthetic perovskite enriched to 95% ^{29}Si revealed exponential spin-lattice relaxation, and hence rapid spin diffusion.[41]

We have dismissed spin diffusion as a viable relaxation mechanism in our orthosilicate systems.[40] Consequently, the theory behind the spin diffusion mechanism will not be dealt with in detail in this work; reference 14 gives a good and highly mathematical treatments of the subject.

Thus, we are left to conclude that all of the spin-lattice relaxation phenomena we observe in orthosilicates are due to electron-nuclear dipolar interactions.

(D) Spin-Lattice Relaxation Behaviour

The investigation of the spin-lattice relaxation behaviour in our synthetic orthosilicates occupied the greatest part of our experimental effort in terms of instrument time consumed. It was, in fact, the bottleneck in our work. The numerical data

obtained for our sol-gel samples and the single precipitated-forsterite sample we looked at, are presented in the Results section.

It has been determined that in the case of 1/2-power stretched exponential spin-lattice relaxation, the inversion recovery experiment requires $D_1 = 21T_{0.5} - 28T_{0.5}$ for 98% - 99% recovery of peak height.

Consider the ideal case for inversion recovery:

$$M_z=M_o\{1-2\exp[-(\frac{t}{T_n})^n]\} \quad (28)$$

$$M_z=M_o-2M_o\exp[-(\frac{t}{T_n})^n] \quad (29)$$

$$Y=\frac{M_o-M_z}{2M_z} \quad (30)$$

The general equation for Y then becomes:

$$Y=\exp[-(\frac{t}{T_n})^n] \quad (31)$$

For 99% recovery of peak height, we must set Y=0.005.

In the case of exponential behaviour, we have n=1, and find that:

$$t_{99\%rec.}=5.3T_1 \quad (32)$$

In the case of 1/2-power stretched-exponential behaviour, we have n=0.5, and find that:

$$t_{99\%rec.}=28.1T_{0.5} \quad (33)$$

If an insufficiently long D_1 value is used in the inversion recovery program, the value of n will be increased such that $0.5 < n < 1$, and the apparent spin-lattice relaxation time T_n may be shorter than its true value. In the case of our own work, the lack of a universal consensus in the literature as to the general nature of spin-lattice relaxation in systems of our type[3,11-14,16,40,42] led to a delay in our appreciation of how long the delays we were using should be. These delays are in fact enormous, and consequently obtaining even one measurements requires huge amounts of instrument time.

Turning to the numerical aspect of our measurements, we must consider 3 aspects: (i) possible background contamination which could distort relaxation times, (ii) the relation governing the relaxation time and the concentration of paramagnetics, and (iii) the relative relaxational efficiencies of the 3 dopants in the forsterite and willemite structures.

(1) Background Contamination

As we are not interested in identifying any or all possible contaminants, but rather care only about their effect on our spin-lattice relaxation measurements, undoped forsterite and willemite were examined for their background spin-lattice relaxation times. The relaxation times proved for too long to measure accurately, but we were able to get minimum values (see Tables 4 and 5); we therefore ruled out any observable spin-lattice relaxation effects due to contamination of our magnesium and zinc nitrate, TEOS, and ethanol.

(2) Relation Governing T_n and $[M^{2+}]$

$$\frac{1}{T_{1obs.}} = \frac{1}{T_{1paramagnetic}} + \frac{1}{T_{1background}} \qquad 34$$

T_1 should be inversely proportional to the concentration of paramagnetic impurities-the question then arises if this is also true for $T_{0.5}$? Our experimental data do bear out this correlation in many instances, albeit not quite as well as we would like. This is due either to large experimental errors, the physical properties of the minerals themselves, or both. The implication is that the relaxation rate is directly proportional to the concentration of paramagnetic centres, regardless of the precise nature of the relaxation law.

(3) Relative Relaxational Efficiencies of Co(II), Ni(II), and Cu(II)

The most difficult problem remaining to be addressed is that of the relative relaxational efficiencies of Co(II), Ni(II), and Cu(II) in forsterite and willemite. This is difficult to address with certainty due to (i) the relative incompleteness of the willemite data, and (ii) the possibility that the transition metal may have a nonrandom distribution within the lattice or may actually form a second orthosilicate phase too minor to be picked up by the XRD analysis. Also of interest, is that the cation (II) sites in forsterite are distorted octahedral (2 types) and in willemite they are distorted tetrahedral.

The relaxation time versus transition metal concentration data for our synthetic forsterites is displayed graphically in Figure 11-14. Examining the forsterite data for copper doping, the most obvious feature is the pronounced nonlinearity of the curve: this corresponds to an apparent increase in the relaxational efficiency of Cu(II) with increasing concentration. There is no obvious mechanism to explain this process.

The nickel forsterites exhibit apparent very efficient relaxational properties over the entire range of concentrations examined. It is suspected that Ni(II) forsterites are a 2 solid phase system as well, the phases being, in the case of low nickel concentrations, Mg_2SiO_4 and $(Mg_x,Ni_y)_2SiO_4$.[24] The authors of reference 24 base this conclusion on what are described on anomolies in the cell parameters. Thus relaxation may appear to be more efficient than it inherently is because the concentration of Ni(II) in the phase being observed is much higher than assumed. The overall curve shape is similar to that for the Cu(II)-doped forsterites.

The cobalt forsterite data must remain suspect, as the fixed delay in the inversion recovery experiment was invariably much too short. Nonetheless, as the magnitude of the error was comparable in each case, we have presented the data. It appears that the linear correlation is reasonably good, although the lack of a point at dopant levels greater than 10% may mask the similarity to the other forsterite curves.

As there may be a structural factor involved, no firm conclusions can be drawn about the innate relative relaxational

FIGURE 11

Inverse Spin-Lattice Relaxation Time versus Dopant Ion Concentration for Forsterite

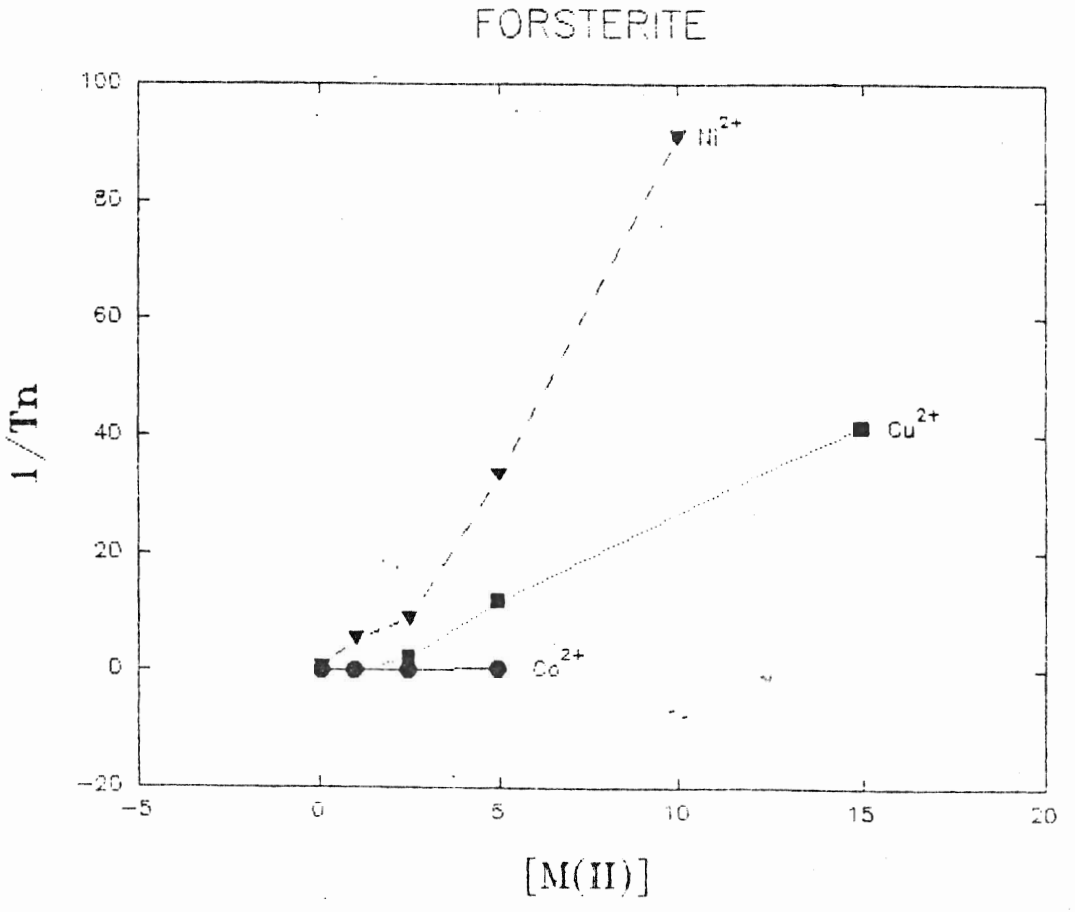

FIGURE 12

Inverse Spin-Lattice Relaxation Time versus Co^{2+} Concentration for Forsterite

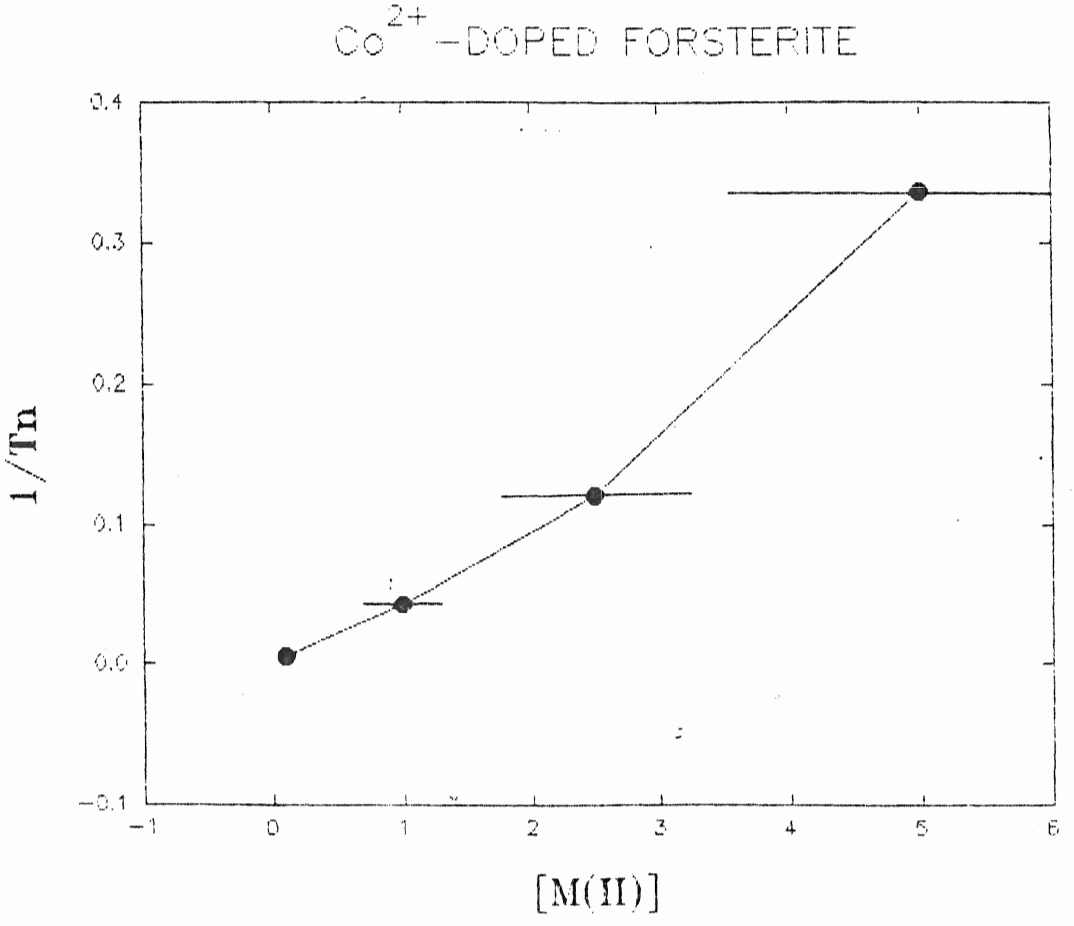

FIGURE 13

Inverse Spin-Lattice Relaxation Time versus Ni^{2+} Concentration for Forsterite

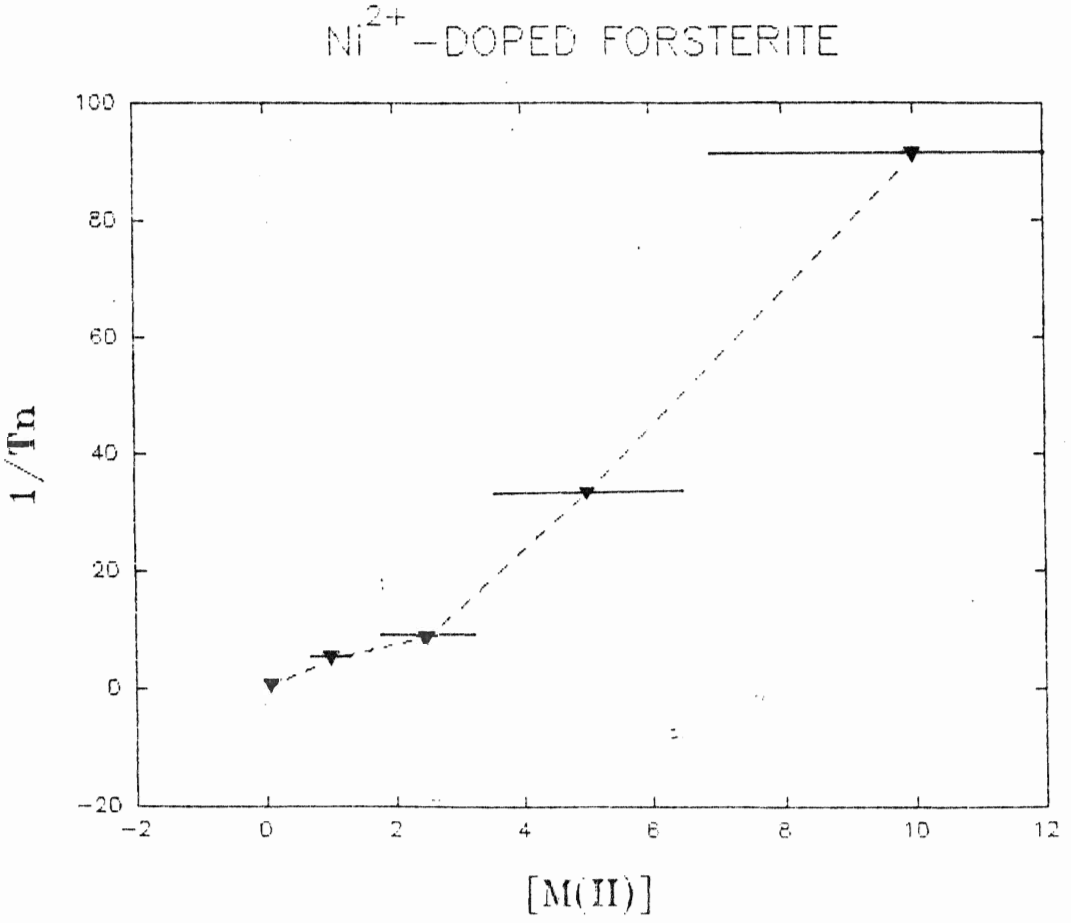

FIGURE 14

Inverse Spin-Lattice Relaxation Time versus Cu^{2+} Concentration for Forsterite

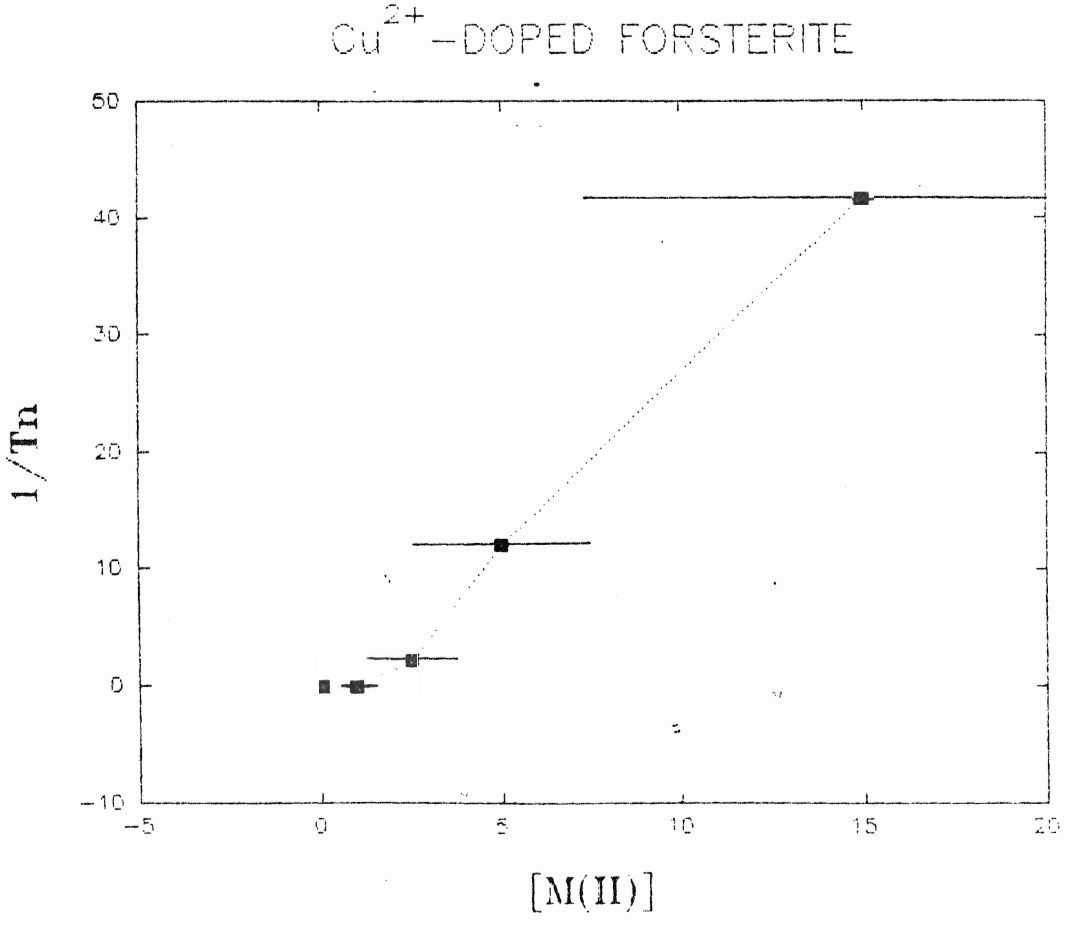

efficiencies of Co(II), Ni(II), and Cu(II) in forsterite. However, the apparent relaxational efficiencies are Ni(II) > Cu(II) > Co(II).

We now turn to the synthetic willemites (Figures 15-18). In the case of the copper system, although the relative fixed delays vary widely, there is a reasonably good linear correlation between the spin-lattice relaxation time and the concentration of the paramagnetic impurity. Likewise, the cobalt willemite system displays a reasonable linearity as predicted by theory (although the data is by no means ideal).

The nickel willemite is puzzling; we only have 2 measurements, and so cannot comment about linearity. However, we can say that the relaxation times are very long. This indicates a deactivation of Ni(II) as a spin-lattice relaxation agent in synthetic willemite; one possible cause is the formation of a nickel-rich, nonsilicate mineral phase. The nickel ion site in willemite itself is distorted tetrahedral: the Ni(II) should be paramagnetic in this configuration. The discrepancy between the apparent spin-lattice relaxational efficiency of Ni(II) in forsterite and willemite is extreme, and adds credence to our suspicion that the nickel-willemite system is not a simple one phase system.

Again, for the reason stated above, we are unable to reach any firm conclusions about the relative relaxational efficiencies of Co(II), Ni(II), and Cu(II) in willemite, although the apparent relaxational efficiencies are Co(II) >> Cu(II) > Ni(II).

Recall that the relation governing relaxation of a nucleus

FIGURE 15

Inverse Spin-Lattice Relaxation Time versus Dopant Ion Concentration for Willemite

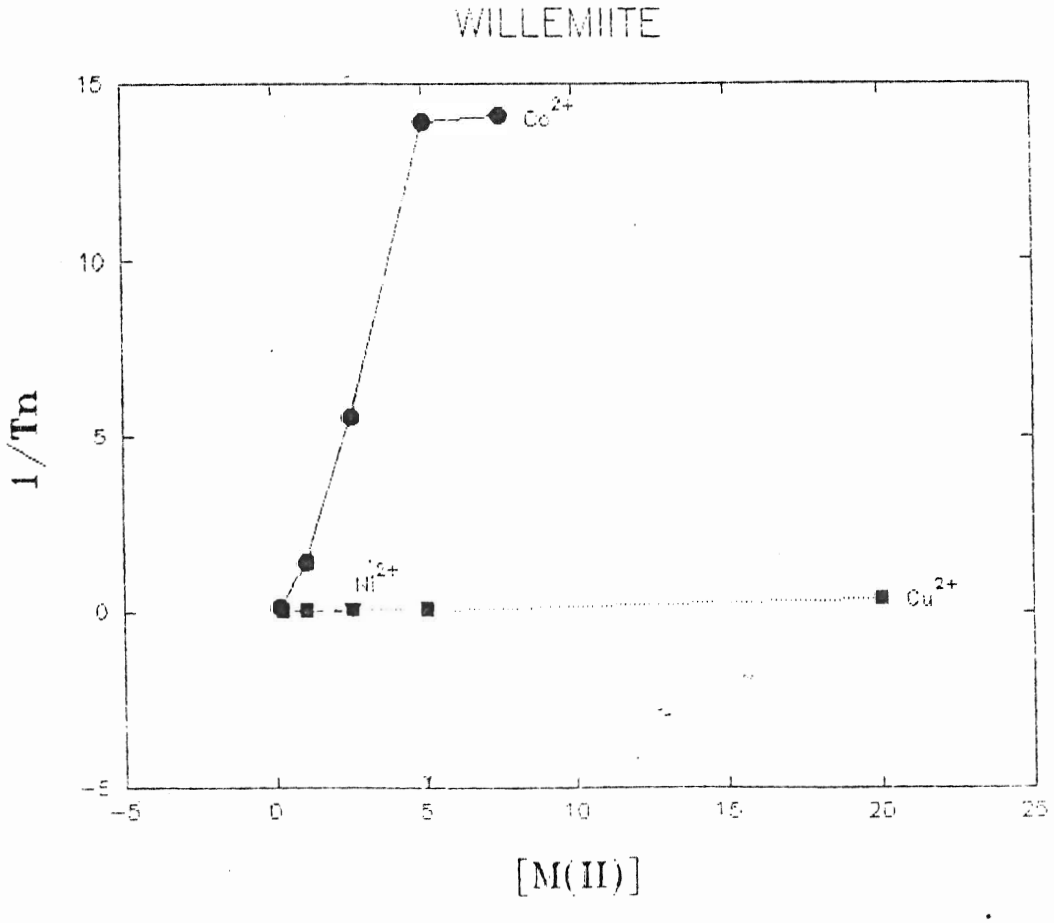

FIGURE 16

Inverse Spin-Lattice Relaxation Time versus Co^{2+} Concentration for Willemite

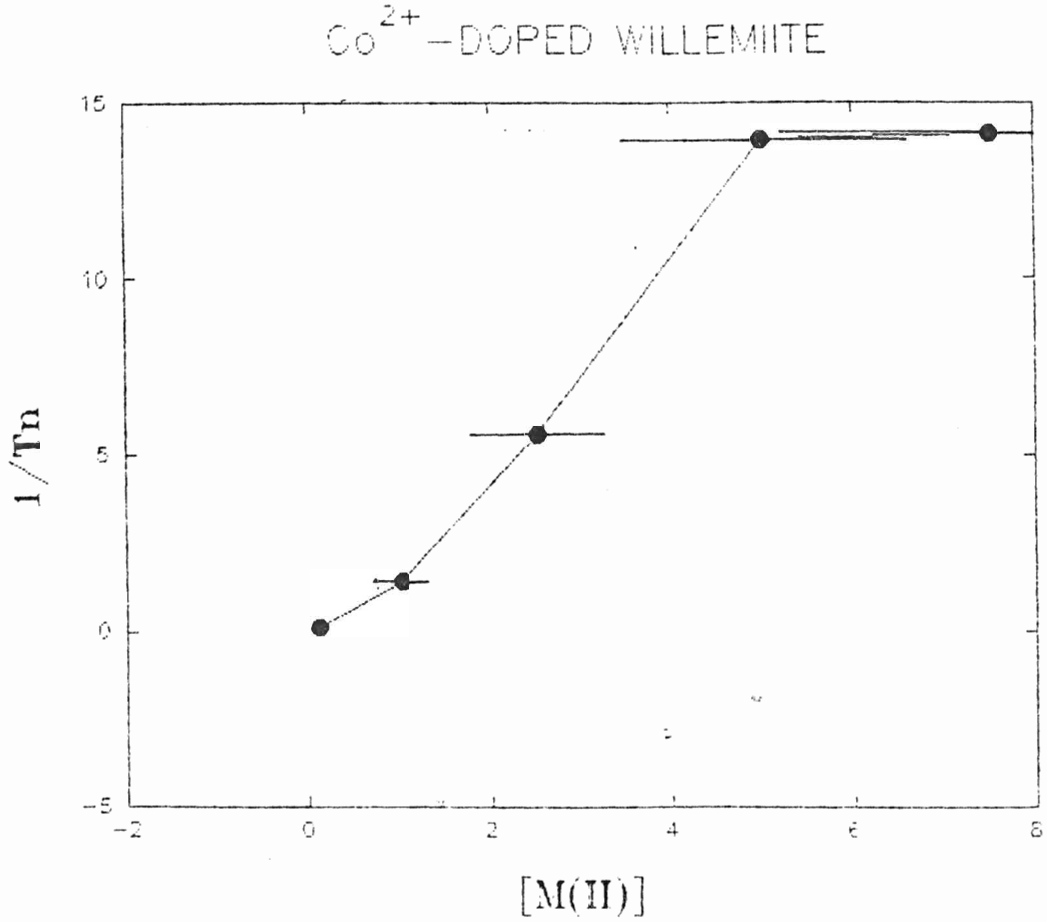

FIGURE 17

Inverse Spin-Lattice Relaxation Time versus Ni^{2+} Concentration for Willemite

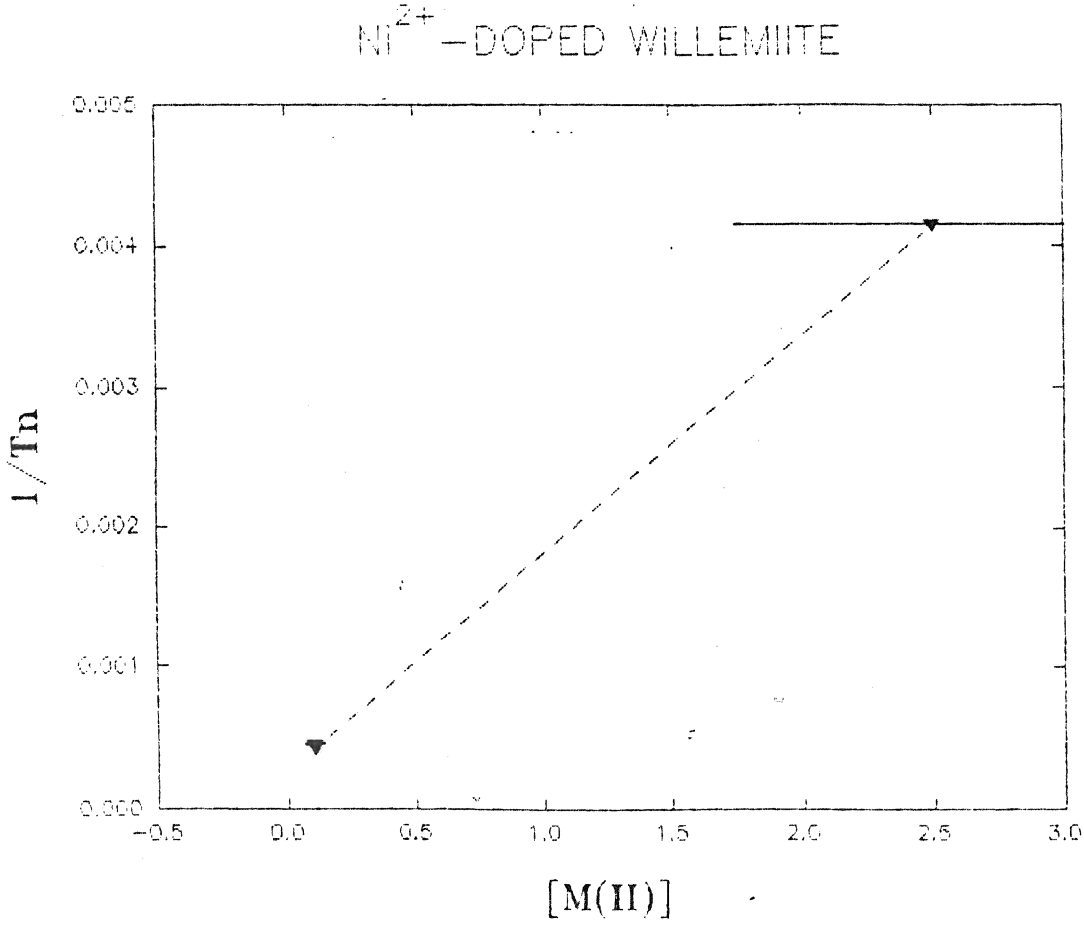

FIGURE 18

Inverse Spin-Lattice Relaxation Time versus Cu^{2+} Concentration for Willemite

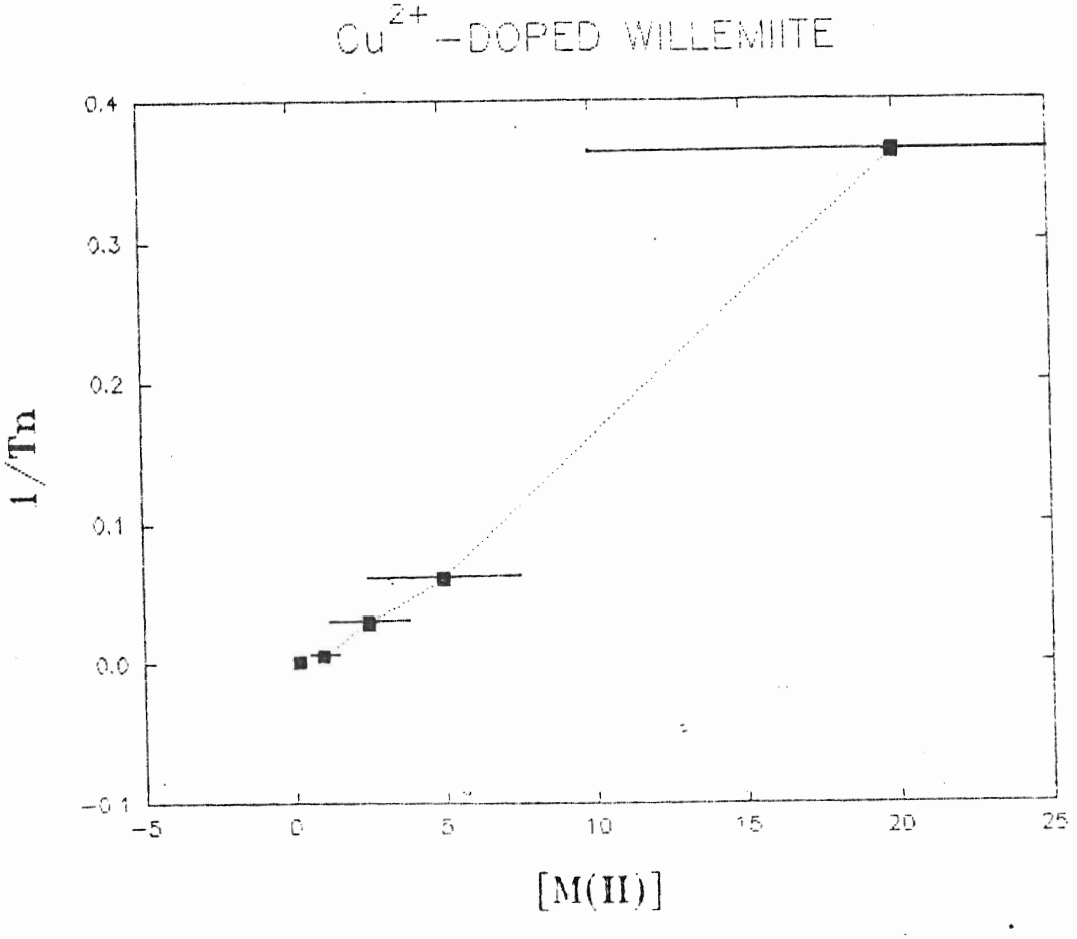

by an unpaired electron contains the relaxation time of the electron:

$$\left(\frac{\tau}{1+\omega_I\tau^2}\right) \qquad 35$$

As this expression is related to the rest of the equation by multiplication, it has a significant bearing on the nuclear spin-lattice relaxation time. There will be some optimum electronic relaxation time, for which the spin-lattice relaxation process will be most efficient. For very short or very long electronic relaxation times, the above expression essentially vanishes and spin-lattice relaxation becomes a very lengthy process. The unknown is how the electronic relaxation time is affected by the distortions in the tetrahedral and octahedral sites that the paramagnetic ions occupy. Thus we have another factor contributing to the spin-lattice relaxation times, which we cannot quantify.

(E) Theoretical Models

The search for a theoretical model to explain the spin-lattice relaxation behaviour observed for our synthetic orthosilicates was not straightforward.

Early in our research, we noticed that the best-fit exponential regression curve which the Aspect 3000 computer was fitting to our inversion recovery experimental data points was not the proper function. After consulting the literature and considering the problem carefully, we tentatively concluded that our relaxation data followed a stretched-exponential pathway: $Y=\exp[-(t/T_n)^n]$.[43]

Once we came to terms with this fact, the search was on for a function which would properly describe our data. We considered a sum of exponentials, typically 2 or 3 individual expressions, to describe the data. Although they fit is satisfactory, there is no basis for choosing a particular number of exponentials to describe the inversion recovery: the regression parameters appear to have no physical meaning.

A stretched-exponential was next considered as this type of relaxation behaviour had been observed previously.[14] Ironically, a sum of exponentials can, if properly distributed, mimic a stretched-exponential quite closely. Thus, we reached a point where we routinely used a stretched-exponential regression function -- 4-parameter of the type:

$$Y=A3+A2*\exp\left[-\left(\frac{t}{T_n}\right)^n\right] \qquad \textbf{36}$$

fully suspecting that the system was actually undergoing longitudinal relaxation describing the sum of a very large number of exponentials. The T_n thus would represent a bulk relaxation time, with n being a measure of the width of the distribution of individual nuclear relaxation times.

The 1/2-power stretched-exponential is occasionally mentioned in the literature[44,45,46,47], but is virtually always presented as an empirical function, with no mention made of its origins. The exception is the paper by Shlesinger and Klafter, which details the generation of the stretched-exponential function, and provides the basis for deriving the 1/2-power bias in the stretch-parameter n.[11]

CONCLUSIONS

In every case, we observed stretched-exponential spin-lattice relaxation. Where the fixed delay in the inversion recovery sequence was sufficiently long, there was a clear tendency for n to be approximately 0.5 +/- 0.1 (the estimated error). Genuine deviations from half-power are observed for several samples containing greater than or equal to 2.5% dopant. As we have a comprehensive theoretical argument in favour of 1/2-power stretched-exponential spin-lattice relaxation behaviour, any deviation must be related to the nonapplicability of the derivation. We suggest two possible areas for deviation: the theory assumes a random distribution of paramagnetic ions, but we have no proof that it is in fact random, as some sort of fractal distribution is equally viable. Secondly, there is an assumption of low paramagnetic ion concentration; beyond a certain, as yet undefined concentration, this condition breaks down and subsequent approximations made on this basis are invalidated.

Many of our synthetic orthosilicates are complex systems. The most striking evidence of this is the deviation from a direct proportionality between spin-lattice relaxation rates and paramagnetic dopant concentration. In some cases this may be experimental error, but is obviously genuine in the case of copper doped forsterites. For the nickel doped forsterites there is independent evidence from the literature of 2 solid phases. This has precluded any firm conclusions about the innate relative relaxational efficiencies of Co(II), Ni(II), and Cu(II) in synthetic forsterite and willemite.

REFERENCES

1. D. Shaw, "Studies in Physical and Theoretical Chemistry Vol. 30-Fourier Transform N.M.R. Spectroscopy-2nd edition," Elsevier, especially 1-5, 167-169, chapter 9 (1984).

2. R.M. Silverstein, G.C. Bassler, T.C. Morrill, "Spectrometric Identification of Organic Compounds-3rd Edition," John Wiley and Sons, Inc., 162-163 (1974).

3. A. Abragam, "The Principles of Nuclear Magnetism," Oxford at the Clarendon Press, 103-106, 306, 380, 382 (1961).

4. C.A. Fyfe, "Solid State NMR for Chemists," C.F.C. Press (1983).

5. F.C. Hawthorne (editor), "Reviews in Mineralogy Volume 18-Spectroscopic Methods in Mineralogy and Geology," Mineralogical Society of America, chapter 8 (F.C. Hawthorne), and 9 (J.R. Kirkpatrick) (1988).

6. M. Magi, E. Lippmaa, A. Samoson, G. Engelhardt, A.-R. Grimmer, J. Phys. Chem., 88, 1518-1522 (1984).

7. E. Breitmaier, W. Voelter, "Carbon-13 NMR Spectroscopy-High-Resolution Methods and Applications in Organic Chemistry and Biochemistry-Third, completely revised edition," VCH, 5,6 (1987).

8. "Bruker Aspect 3000 NMR Software Manual," section 1- page1, section 19-page 27, section 33-page 70, section 48-page 62 (1985).

9. H. Scher, M.F. Shlesinger, J.T. Bendler, Physics Today, 44, 26-34 (1991).

10. E.W. Montroll, J.T. Bendler, J. Stat. Phys., 34, 129 (1984).

11. L. Pietronero, E. Tosatti (editors), "Fractals in Physics," Elsevier (1986).
M.F. Shlesinger, J. Klafter, "The Nature of Temporal Hierarchies Underlying Relaxation in Disordered Systems," 393-398.

12. W.E. Blumberg, Phys. Rev., 119(1), 79-84 (1960).

13. D. Tse, S.R. Hartmann, Phys. Rev. Lett., 21(8), 511-514 (1968).

14. B. Maiti, B.R. McGarvey, J. Magn. Reson., 58, 37-46 (1984).

15. A. Thangaraj, S. Ganapathy, Indian Journal of Chemistry, 29A, 1080-1082 (1990).

16. F. Devreux, J.P. Boilot, F. Chaput, B. Sapoval, Phys. Rev. Lett., 65(5), 614-617 (1990).

17. P.F. Barron, P. Slade, R.L. Frost, J. Phys. Chem., 89, 3305-3310 (1985).

18. D.J. Cookson, B.E. Smith, J. Magn. Reson., 63, 217-218 (1985).

19. J. Klinowski, T.A. Carpenter, J.M. Thomas, J. Chem. Soc., Chem. Commun., 956-958 (1986).

20. M.J.R. Hoch, E.C. Reynhardt, Phys. Rev. B, 37(16), 9222-9226 (1988).

21. R. Lenk, "Studies in Physical and Theoretical Chemistry Vol. 43-Fluctuations, Diffusion and Spin Relaxation," Elsevier, 63-71 (1986).

22. J.S. Hartman, M. Seifried (1986), results unpublished.

23. E. Fukushima, S.B.W. Roeder, "Experimental Pulse NMR-A Nuts and Bolts Approach," Addison-Wesley Publishing Company Inc., 136-157 (1981).

24. W.A. Deer, R.A. Howie, J. Zussman, "Rock-Forming Minerals, Vol. 1A, 2nd edition-Orthosilicates, Longman Group Limited, 2-5, 8 (1982), and references contained therein.

25. W. Eitel, "The Physical Chemistry of the Silicates," The University of Chicago Press, 22 (1954), and references contained therein.

26. C. Hang, M.A. Simonov, N.V. Belov, Soviet Physics-Crystallography, 15(3),387-390 (1970).

27. W.L. Bragg, W.H. Zachariasen, Z. Kristallogr., 72, 518-528 (1930).

28. L.L. Hench, D.R. Ulrich (editors), "Science of Ceramic Chemical Processing," John Wiley and Sons Inc. (1986).

29. J.D. Mackenzie, D.R. Ulrich, "Ultrastructure Processing of Advanced Ceramics," John Wiley and Sons Inc., chapter3, 7, 11, 20, 23, 65, and referenced contained in chapter 3 (1988).

30. C.J. Brinker, G.W. Scherer, "Sol-Gel Science," Academic Press, Inc. (1990).

31. H.H. Willard, L.L. Merritt Jr., J.A. Dean, F.A. Settle Jr., "Instrumental Methods of Analysis-Sixth Edition," Wadsworth Publishing Company, Section 9.8 (1981).

32. A. Kazakos, S. Komarneni, R. Roy, Materials Letters, 9(10), 405-409 (1990).

33. K. Yukigiro, Y. Tamotsu, Denke Kagaku oyobe Kogyo Butsuri Kagaku, 53(10), 831-833 (1985).

34. G.W. Ewing, "Instrumental Methods of Chemical Analysis-Fifth Edition," McGraw-Hill Book Company, 200-202 (1985).

35. N.A. Ball, personal communication.

36. G.M. Bancroft, P.G.L. Williams, E.J. Essene, Mineralogical Society of America Special Paper, 2, 59-65 (1969).

37. R.C. Weast, "Handbook of Chemistry and Physics-59th Edition,"CRC Press, B-112, B-116, B-141 (1978).

38. S. Borman, Chem. and Eng. News, Science/Technology, 28-35 (Apr.22, 1991).

39. B.L. Sherriff, J.S. Hartman, Canadian Mineralogist, 23, 205- 212 (1985).

40. I. Farnan, J.F. Stebbins, J. Am. Chem. Soc., 112, 32-39 (1990).

41. R.J. Kirkpatrick, D. Howell, B.L. Phillips, X.-D. Cong, E. Ito, A. Navrotsky, American Mineralogist, 76, 673-676 (1991).

42. T. Watanabe, H. Shimizu, A. Masuda, H. Saito, Chem. Lett., 1293-1296 (1983).

43. P. Bordewijk, Chem. Phys. Lett., 32(3), 592-596 (1975).

44. W. Seibrand, T.A. Wildman, Acc. Chem. Res., 19, 128 (1986).

45. H. Scher, M.F. Schlesinger, J.T. Bendler, Physics Today, 44, 26 (1991).

46. W. Seibrand, T.A. Wildman, Int. Revs. Phys. Chem., 5, 251 (1986).

47. P.M. Henrichs et al, J. Magn. Reson., 58, 85 (1984).